



1 **Ultradian rhythms in shell composition of photosymbiotic and non-photosymbiotic**
2 **mollusks**

3 Niels J. de Winter^{1,2}, Daniel Killam³, Lukas Fröhlich⁴, Lennart de Nooijer⁵, Wim Boer⁵, Bernd R.
4 Schöne⁴, Julien Thébault⁶, Gert-Jan Reichart^{2,5}

5

6 *Affiliations*

7 ¹Analytical, Environmental and Geochemistry group (AMGC), Vrije Universiteit Brussel, Brussels,
8 Belgium

9 ²Dept. of Earth Sciences, Utrecht University, Utrecht, the Netherlands

10 ³ San Francisco Estuary Institute, Richmond, CA, USA

11 ⁴ Department of Paleontology, Institute of Geosciences, Johannes Gutenberg Universität, Mainz,
12 Germany

13 ⁵ Dept. of Ocean Systems, Royal Netherlands Institute for Sea Research (NIOZ), Texel, the
14 Netherlands

15 ⁶Univ Brest, CNRS, IRD, Ifremer, LEMAR, 29280 Plouzané, France, (ORCID: 0000-0002-3111-
16 4428)

17

18 Corresponding author: N.J. de Winter, niels.de.winter@vub.be

19



20 **Abstract**

21 The chemical composition of mollusk shells is a useful tool in (paleo)climatology since it captures
22 inter- and intra-annual variability in environmental conditions. Trace element and stable isotope
23 analyses with improved sampling resolution now enable the use of mollusk shells for
24 paleoenvironmental reconstructions at a daily to sub-daily resolution. Here, we discuss hourly
25 resolved Mg/Ca, Mn/Ca, Sr/Ca and Ba/Ca profiles measured by laser ablation ICP-MS through
26 shells of photosymbiotic giant clams (*Tridacna maxima*, *Tridacna squamosa* and *Tridacna*
27 *squamosina*) and the non-photosymbiotic scallop *Pecten maximus*. Precise sclerochronological
28 age models and spectral analysis allowed us to extract daily and tidal rhythms in the trace element
29 composition of these shells. We find significant expression of these periodicities but conclude that
30 this cyclicity explains less than 10% of the sub-annual variance in trace element profiles. Tidal
31 and diurnal rhythms explain variability of at most 0.2 mmol/mol (~10% of mean value) in Mg/Ca
32 and Sr/Ca, while Mn/Ca and Ba/Ca cyclicity has a median amplitude of less than 2 $\mu\text{mol/mol}$
33 (~40% and 80% of the mean of Mn/Ca and Ba/Ca, respectively). Daily periodicity in Sr/Ca and
34 Ba/Ca is stronger in *Tridacna* than in *Pecten*, with *Pecten* showing stronger tidal periodicity. One
35 *T. squamosa* specimen which grew under a sunshade exhibits some of the strongest diurnal
36 cyclicity. Daily cycles in trace element composition of giant clams are therefore unlikely to be
37 driven by variations in direct insolation itself but reflect an inherent biological rhythmic process
38 affecting element incorporation. Finally, the large amount of trace element variability unexplained
39 by periodic variability highlights the dominance of aperiodic processes in mollusk physiology
40 and/or environmental conditions on shell composition at the sub-daily scale. Future studies should
41 aim to investigate whether part of this aperiodic variability in shell chemistry reliably records
42 weather patterns or circulation changes in the paleoenvironment.

43

44 **1. Introduction**



45 Patterns in growth increments, microstructure, and chemical composition of accretionary
46 carbonate bioarchives yield detailed information about the environmental conditions and
47 biological rhythm of carbonate producing animals (Dunbar and Wellington, 1981; Jones, 1983;
48 Witbaard et al., 1994; Klein et al., 1996; Surge et al., 2001; Schöne et al., 2005a; Ivany, 2012;
49 Schöne and Gillikin, 2013; DeCarlo and Cohen, 2017; Killam and Clapham, 2018). These
50 characteristics have spurred the development of a multitude of techniques for extracting
51 information about life history (Jones and Quitmyer, 1996; Schöne et al., 2005b; Goodwin et al.,
52 2009; Mahé et al., 2010; Comboul et al., 2014; DeCarlo and Cohen, 2017; Judd et al., 2018; de
53 Winter, 2022), carbonate chemistry (Sinclair et al., 1996; Lazareth et al., 2003; Schöne et al.,
54 2010; de Winter and Claeys, 2017; Warter and Müller, 2017; Huyghe et al., 2021; de Winter et
55 al., 2021a) and microstructure (Lazier et al., 1999; Checa et al., 2007; Popov, 2014; Gilbert et al.,
56 2017; Crippa et al., 2020; Höche et al., 2020; 2021; Wichern et al., 2022) from carbonate shells
57 and skeletons. As a result, (fossil) carbonate skeletons have gained much attention as archives
58 of past environmental and climate change (e.g., Lough, 2010; Schöne and Gillikin, 2013; Ivany
59 and Judd, 2022 and references therein).

60 Three characteristics make the shells of marine mollusks especially valuable as climate archives:
61 (1) Nearly all marine mollusks precipitate their shells in isotopic equilibrium with ambient sea
62 water, except for juvenile oysters and some mollusks growing near hydrothermal vents (Schöne
63 et al., 2004; Wisshak et al., 2009; Huyghe et al., 2021; de Winter et al., 2022), (2) mollusk shells
64 have a high fossilization potential and long geological history, dating back to the beginning of the
65 Phanerozoic (Al-Aasm and Veizer, 1986a; b; Jablonski et al., 2003; Cochran et al., 2010;
66 Jablonski et al., 2017; de Winter et al., 2017; 2018; Coimbra et al., 2020), (3) the incremental
67 growth of mollusk shells allows for internal dating within the shell, yielding chronologies of shell
68 growth with sub-annual precision (Richardson et al., 1980; Jones, 1983; Schöne et al., 2005c;
69 Goodwin et al., 2009; Huyghe et al., 2019). These advantages enable mollusk shells to record



70 important information about climate and ambient water chemistry on the seasonal scale. Thereby,
71 reconstructions from mollusk shells are highly complementary to other, less highly resolved but
72 longer-term, climate and environmental reconstructions like sedimentary records, tree rings and
73 ice cores (Black, 2009; Bougeois et al., 2014; Petersen et al., 2016; Tierney et al., 2020; de Winter
74 et al., 2021b).

75 The resolution of the mollusk shell archive is not limited to seasonal variability. Studies monitoring
76 the behavior of mollusks during growth experiments show that their activity varies as a function
77 of environmental conditions (e.g., temperature and food availability) and follows ultradian rhythms
78 which may contain daily to hourly periodicities, probably linked to diurnal and tidal cycles, or lack
79 periodic behavior altogether (Rodland et al., 2006; García-March et al., 2008; Tran et al., 2011;
80 Ballesta-Artero et al., 2017; Xing et al., 2019; Tran et al., 2020). Analyses of growth patterns and,
81 more recently, composition of shell carbonate deposited at these short time intervals show that
82 these rhythms can be recorded in mollusk shells (Pannella, 1976; Richardson et al., 1980; Sano
83 et al., 2012; Warter et al., 2018; de Winter et al., 2020). This raises the question whether mollusk
84 shells reliably record behavioral changes, high frequency (paleo-) weather or circulation patterns
85 (e.g., Komagoe et al., 2018; Yan et al., 2020; Poitevin et al., 2020). Alternatively, the presence of
86 daily cyclicity in shell chemistry may yield information about the paleobiology of extinct mollusks,
87 such as the presence of photosymbiosis (e.g., Sano et al., 2012; Warter et al., 2018; de Winter et
88 al., 2020). The latter seems plausible given the effect of photosymbiosis on shell mineralization
89 in modern tridacnids (Ip and Chew, 2021) and on the trace element composition of aragonite in
90 modern photosymbiotic scleractinian corals (Cohen et al., 2002; Meibom et al., 2003; Inoue et al.,
91 2018). If proven true, daily variability in bivalve shells may serve as a proxy for photosymbiosis in
92 the fossil record (e.g., de Winter et al., 2020). This is of interest because photosymbiosis is a
93 derived adaptation of some tropical bivalve species (e.g., tridacnids) and its prevalence in the
94 fossil record has important implications for the ecological niche of fossil mollusks (e.g., Vermeij,



95 2013). In addition, photosymbiosis can affect mollusk shell composition, and understanding it is
96 therefore critical for the interpretation of chemical proxies in mollusk shells for environmental
97 reconstructions (Killam et al., 2020). Finally, improving our understanding of photosymbiosis in
98 tropical ecosystems sheds light on the resilience of photosymbiotic organisms to environmental
99 change, now and in the geological past. The latter is of special interest in light of the ongoing
100 climate and biodiversity crises, which are profoundly affecting these sensitive ecosystems
101 (Pandolfi and Kiessling, 2014).

102 In this study, we investigate shell growth patterns and shell chemistry of the photosymbiotic
103 bivalves *Tridacna maxima*, *T. squamosa* and *T. squamosina* as well as the non-photosymbiotic
104 scallop *Pecten maximus*. *P. maximus* was chosen as a non-photosymbiotic counterpart in
105 comparison with the tridacnids because of its comparatively high growth rate and the presence of
106 daily striae on the outside of its shell, which make it possible to construct accurate shell
107 chronologies (Chauvaud et al., 2005). We combine ultra-high-resolution (hourly resolved) Mg/Ca,
108 Sr/Ca, Mn/Ca and Ba/Ca measurements in the shells with detailed sclerochronology to investigate
109 the variability in these trace elements over time in all four species. The aim of this study is to
110 investigate (1) whether the shells record high-frequency variability in shell chemistry that can be
111 linked to environmental and/or circadian rhythms and (2) whether the presence of photosymbiosis
112 influences the expression of this variability in the shells' composition.

113



114 **2. Materials and methods**

115 2.1 Preparation of *P. maximus* specimens

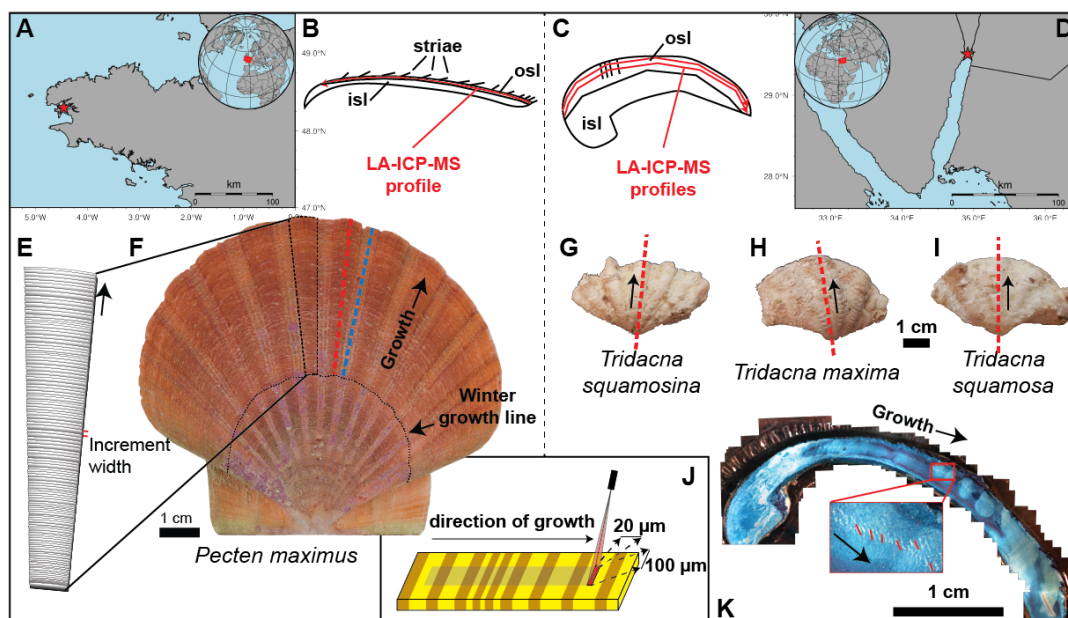
116 Three specimens of the King scallop *P. maximus* (labeled “PM2”, “PM3” and “PM4”) were
117 collected alive on 15/11/2019 on the southern coast of the Bay of Brest near Lanvéoc, France
118 (48°17'N 4°30'W) by SCUBA divers at a depth of approximately 8 m (see Fröhlich et al., 2022;
119 **Figure 1**). Note that water depth in the Bay of Brest varies significantly due to the macrotidal
120 regime with a mean tidal range of 2.8 – 5.9m with extreme ranges up to 7.2m (Guillaume-Olivier
121 et al., 2021; Service Hydrographique et Océanographique de la Marine; 2022). Collected
122 specimens contained at least one full year of growth based on the visibility of one winter growth
123 line on the outside of the shell (age class 1; see Thébault et al., 2022 ; **Fig 1F** and **S1**). Specimens
124 were frozen at -20°C immediately after collection. Soft body parts and epibionts were removed
125 from the shells before further treatment. Shells were superficially cleaned using a plastic brush
126 and adhering sediment was removed by ultrasonication in deionized water. The flat, left valves
127 were used for elemental and sclerochronological analysis following previous studies on *P.*
128 *maximus* (Thébault et al., 2022; Fröhlich et al., 2022).

129 High-resolution color photos were made of the outside of the left valve of the shell using a mirror-
130 reflex camera (Canon EOS 600 DSLR camera connected to a Wild Heerbrugg binocular
131 microscope equipped with a Schott VisiLED MC 1000 light source) aimed downward
132 perpendicular to the working surface. Overlapping images of the shells were stitched together
133 using Image Composite Editor v2.0.3.0 (Microsoft Research Computational Photography Group,
134 Redmond, WA, USA). The stitched images were used to count and measure daily striae on the
135 shell surface (see **Fig. 1** and **S1**). To obtain a fully focused composite of the complete shell,
136 dynamic focusing was applied to allow all parts of the slightly curved surface of the shell to come
137 into focus. Dynamic focus images were later stitched together using focus stacking in Helicon
138 Focus (Helicon Focus 7.7.5; HeliconSoft, Kharkiv, Ukraine; see **S1**).



139 Cross sections were cut through all three *P. maximus* shells perpendicular to the daily growth
140 lines (striae) from the ventral margin of the shell to the shell hinge (see **Fig. 1B**, **Fig. 1E-F** and
141 **S1**) along the axis of maximal growth. Shells were fortified with a protective layer of metal epoxy
142 (Gluetec Wiko Epofix 05) before sectioning using a Buehler Isomet 1000 low-speed precision saw
143 (Buehler Inc, Lake Bluff, IL, USA) equipped with a diamond-coated wafering thin blade (0.4 mm
144 thickness; number 15LC 11–4255) at 200 rpm. Parallel cuts were made to allow shell sections to
145 be glued to glass plates for high-grade polishing (down to F1200 grit SiC powder and 1 μm Al_2O_3
146 suspension). Two cross sections were made through specimens **PM2** and **PM3**: One through a
147 “rib” of the shell (i.e., radial segment that protrudes away from the interior, named **PM2_1** and
148 **PM3_1**) and one through a “valley” (i.e., radial segment between two “ribs” that lies deeper
149 towards the interior, named **PM2_2** and **PM3_2**; see **Fig. 1** and **S1**). The dual sections were cut
150 to compare shell chemistry between the “ribs” and “valleys” of the shell . Specimen **PM4** was only
151 sectioned once, through a “valley” in the shell, making a total of five cross sections through the *P.*
152 *maximus* specimens.

153



154

155 **Figure 1: Overview of sample locations and preparation steps. A)** Location of the Bay of
 156 Brest, with the red star indicating the sampling location. **B)** Schematic cross section through *P.*
 157 *maximus* showing how the LA-ICP-MS linescan (red line) was positioned within the outer shell
 158 layer (OSL). **C)** Schematic cross section through a tridacnid, illustrating the positions of parallel
 159 LA-ICP-MS line scans (red lines) through these shells within the OSL. **D)** Position of the Gulf of
 160 Aqaba, with the red star indicating the sample location for tridacnids. **E)** Schematic representation
 161 of a segment through the shell of *P. maximus* showing the striae which are deposited daily and
 162 which were counted to establish age models (see also **B**). **F)** Left valve of *P. maximus* (**PM2**)
 163 used in this study, with dashed lines showing the position of cross sections through ribs (red) and
 164 valleys (blue) in the shell. Black arrow indicates growth direction away from the shell hinge. The
 165 black dotted line highlights a winter growth stop. **G-I)** Pictures of (from left to right) *T. squamosa*
 166 (specimen **TSFRS1**), *T. maxima* (specimen **TM29**) and *T. squamosina* (specimen **SQSA1**) with
 167 dashed red lines indicating the positions of the cross sections used for LA-ICP-MS analysis (see
 168 **C**) and black arrows indicating the direction of growth. **J)** Schematic representation of the LA-ICP-



169 MS line scanning setup with the rectangular spot size (100 * 20 μm ; see **S11**) that was positioned
170 parallel to the growth layers in the shell. **K)** Example of Mutvei-stained cross section through a *T.*
171 *maxima* specimen used to visualize and count growth lines, with the insert showing part of the
172 OSL where growth lines were counted (red lines) to establish age models for the tridacnids. Black
173 arrows indicate the direction of growth.

174



175 2.2 Preparation of *Tridacna* specimens

176 A total of 5 tridacnid specimens, two *T. maxima* (named **TM29** and **TM84**), two *T. squamosa*
177 (named **TS85** and **TSFRS1**) and one *T. squamosina* (**SQSA1**) specimen, were collected in the
178 summer of 2016 from beach death assemblages on the coast of the Gulf of Aqaba with permit
179 from the Israeli National Parks Authority (**Figure 1**; see details in Killam et al., 2020). One cultured
180 *Tridacna squamosa* shell (**TSM1**) was obtained from the National Center for Mariculture, Eilat.
181 Species were determined following shell characteristics of the local population as cited in Roa-
182 Quiaoit (2005).

183 All shells were sectioned along the axis of maximum growth after removing epibionts using a
184 metal brush (see **Fig. 1G-I**). Original microstructure and preservation of the original aragonite
185 mineralogy of all specimens was confirmed using Scanning Electron Microscopy and X-ray
186 Diffraction Spectroscopy following Gannon et al. (2017) and Kontoyannis and Vagenas (2000;
187 see details in Killam et al., 2020). Shell segments were partially embedded in Araldite 2020 epoxy
188 resin (Huntsman Corp., Woodlands, TX, USA) before being sectioned in direction of maximum
189 growth using a slow-rotating saw equipped with a thin wafered saw blade ($\varnothing < 1$ mm). Parallel
190 cross sections produced 5-10 mm thick sections that were polished using progressively finer SiC
191 polishing disks.

192

193 2.3 Microscopy and photography

194 Polished surfaces of all 11 cross sections (5 *Pecten*, 6 *Tridacna*) were imaged using an Epson®
195 1850 flatbed scanner (Seiko Epson Corp., Nagano, Japan) at a pixel resolution of 6400 dpi (± 4
196 μm pixel size) as well as by stitching micrographs made using a KEYENCE VHX-5000 digital
197 microscope using x250 magnification together into composite images (see **S1**). Cross sections



198 were imaged both before and after trace element analyses to allow the trace element profiles to
199 be referenced relative to the cross sections.

200

201 2.4 LA-ICP-MS analyses

202 Elemental ratios were based on measuring ratios of the isotopes ^{25}Mg , ^{87}Sr , ^{55}Mn and ^{137}Ba to
203 ^{43}Ca along profiles through all shell cross sections using Laser Ablation – Inductively Coupled
204 Plasma – Mass Spectrometry (LA-ICP-MS). Measurements were carried out on a laser ablation
205 system (ESI NWR193UC; Elemental Scientific, Omaha, NE, USA) coupled to a quadrupole ICP-
206 MS (iCap-Q, Thermo Fisher Scientific, Waltham, MA, USA) at the Royal Netherlands Institute for
207 Sea Research (NIOZ). Operation parameters are provided in **S11**.

208



209

210 Scan lines were programmed on the polished shell cross sections in direction of growth as close
211 as possible to the outer edge of the shell, with the LA-ICP-MS spot oriented parallel to the growth
212 lines (with a width of 20 μm in scanning direction, see **Fig. 1J; S11**). For the pectinids, care was
213 taken to target the outer portion of the outermost shell layer (oOSL) and avoid sampling of the
214 inner portion of the outer shell layer (iOSL) or inner shell layer (ISL), which was demonstrated to
215 have a different chemical composition (see Freitas et al., 2009). For the tridacnids, profiles were
216 placed within the OSL close to (within 100 μm of) the outer edge of the shell in a first analytical
217 session. However, since spikes of high Mg/Ca and Mn/Ca ratios were observed in these results,
218 parallel transects placed \sim 100 μm further towards the inside of the shell were measured through
219 all tridacnid shells to verify whether these spikes in Mg and Mn were reproducible further inward
220 (see **S2**). All scan lines in pectinids and tridacnids were repeated a second time at the exact same
221 location using a faster scan rate of 10 $\mu\text{m}\cdot\text{s}^{-1}$ to assess repeatability of the elemental signals (see
222 **S2**).

223 Data reduction was performed using an adapted version of the data reduction software SILLS
224 (Signal Integration for Laboratory Laser Systems; Guillong et al., 2008) in Matlab. Raw LA-ICP-
225 MS data were calibrated using NIST610, (National Institute of Standards and Technologies,
226 Gaithersburg, MD, USA) using the reference values reported in the GeoReM database (Jochum
227 et al. 2005, 2011). Quality control materials BAS752 (Bureau of Analyzed Samples,
228 Middlesbrough, UK), RS3 and one matrix-matched carbonate standard (MACS-3; United States
229 Geological Survey, Reston, VA, USA; Wilson et al., 2008) were used to monitor the quality of the
230 measurement. To increase the stability of the ICP-MS signal and to correct for drift, ^{43}Ca was
231 used as internal standard. External drift-correction using repeated measurements on the JCp1
232 standard was applied if the element/Ca drift was $>5\%$ during the analytical sequence. Drift during
233 a single transect was found to be negligible.



234

235 2.5 Age models

236 Trace element profiles in *P. maximus* shells were internally dated using daily striae visible on the
237 outer shell surface (**Fig. 1E**). Daily increment widths (perpendicular distances between
238 successive striae) were counted and measured multiple times, both on the outside of the shell
239 using the focus-stacked images (see **section 2.3**) and by counting and measuring the distance
240 between growth layers in cross sections through the “valleys” of the shells (**PM2_2** and **PM3_2**;
241 see **S3**) by different persons. Positions of daily striae on the outside of the shells were plotted
242 relative to distance along the LA-ICP-MS scan line using manual alignment of striae and the LA-
243 ICP-MS path on microscope composites of cross sections through the shells, taking into account
244 the curvature of growth lines with distance away from the outer shell surface (see **S3**). The timing
245 of shell formation was determined by backdating the daily striae from the ventral margin (last
246 visible stria mineralized on the date of shell collection, i.e., November 15, 2019), and by linearly
247 interpolating the timing of measurements located between daily growth lines based on their
248 distance from daily striae positions (**S5**).

249 Trace element profiles from *Tridacna* shells were also dated using layer counting. However, since
250 expression of daily and semi-diurnal growth markings was insufficiently clear to count individual
251 growth lines along the full (multi-year) growth period recorded in all the shells, age models were
252 constructed based on parts of the shell where daily and tidal layers could be identified with
253 confidence. Polished cross sections through all tridacnids were imaged using UV luminescence
254 (see **Fig. 1K** and **S4**) to facilitate this counting. The median widths of daily or semi-diurnal
255 increments were determined on these cross sections and compared to the width of annual
256 increments identified based on growth breaks visible on the outer margin of the shell. The
257 distinction between diurnal (24h) and tidal (~12h) pacing of growth increments was made based
258 on the width of small-scale increments relative to the width of annual increments in the shell. A



259 von Bertalanffy growth model (Von Bertalanffy, 1957) was constructed for each specimen based
260 on the annual growth (ΔL) inferred from growth line counting and the maximum shell height (L_{inf})
261 known for these species in the Red Sea from the literature (Roa-Quiaoit, 2005; Mohammad et al.,
262 2019):

$$263 \quad L_t = L_{inf} * (1 - e^{-kt}), \text{ with } k = -\ln\left(\frac{\Delta L}{L_{inf}}\right)$$

264 In this formula, L_t is the shell height at time t and k is the growth constant (Brody growth coefficient;
265 Munro, 1984). Since cross sections through the tridacnids were made through the shell hinge (in
266 direction of the shell height) and literature values for L_{inf} are reported with reference to shell length
267 (measured parallel to the shell hinge), allometric data on *T. maxima*, *T. squamosa* and *T.*
268 *squamosina* from the literature was used to convert L_{inf} values (which are commonly reported as
269 shell length) to shell height and make them relevant for the direction in which the trace element
270 profiles were measured on the cross sections (Roa-Quiaoit, 2005; Richter et al., 2008;
271 Mohammad et al., 2019). Uncertainties on the annual growth increment widths (ΔL) were
272 calculated from the standard error of the mean width of daily and semi-diurnal growth increments
273 on which ΔL is based, and uncertainties on the values for L_{inf} were taken from variability in the
274 values in the literature. Both sources of uncertainty were propagated through the growth model
275 using the variance formula (Ku, 1966) to obtain error envelopes on age-distance relationships
276 (growth curves) of tridacnids (see **S5**). All data processing steps described in this manuscript are
277 carried out using the open-source computational software package R (R Core Team, 2022), and
278 scripts detailing these calculations are provided in **S6** and deposited on the open-access software
279 repository GitHub (<https://zenodo.org/record/6603175>)

280

281 2.6 Spectral analysis



282 Spectral analysis on the LA-ICP-MS data was used to isolate trace element variability at the sub-
283 annual scale. All trace element profiles were first detrended using a LOESS filter with a span of
284 0.2 times the length of the record to remove longer term (i.e., seasonal to multi-annual) trends.
285 The detrended series were linearly resampled in the time domain before applying the Multi-Taper
286 Method (MTM; Thomson, 1982) to extract dominant frequencies from the data. Spectral analysis
287 was carried out using the “astrochron” package (Meyers, 2014) in R (R Core Team, 2022; see
288 script in **S6**). The significance of relevant periodicities was tested using a combination of “red
289 noise” estimation and a harmonic F-test (see Meyers, 2021). To visualize the evolution of periodic
290 behavior across the shells, wavelet analysis was applied on all trace element profiles using the
291 “dplr” package in R (see **S6**).

292

293 2.7 Extracting high-resolution variability

294 After detrending and spectral analysis, all trace element profiles were smoothed using a Savitzky-
295 Golay filter with a width of 21 datapoints (8.4 μm ; equivalent to a timespan of \sim 1-5h; **S6**) to remove
296 high-frequency measurement noise. Statistically significant (see **section 2.6**) variability in daily
297 (\sim 22-36h; centered on the 24h diurnal cycle) and tidal (\sim 8-14h; centered on the 12.4h tidal cycle)
298 frequency bands was extracted from the trace element records using a combination of bandpass
299 filtering (using the “bandpass” function in the “astrochron” R package) and stacking (see **S6**).
300 Trace element data was stacked along bandpass filters using the following procedure: Maxima
301 and minima in the bandpass filter were used as tie points to reference each datapoint of the
302 smoothed dataset relative to its position within the cycle on a scale from 0 to 1. These relative
303 positions were then used to divide the data into 10 bins (bin 1 contains positions 0 – 0.1, bin 2
304 contains data from positions 0.1 – 0.2, etc.), giving the stacked data a resolution of 0.1 times the
305 length of the cycle under investigation. The full breakdown of variability within and between bins
306 created in the stacking routine is provided in **S7**. Different sources of variance in the trace element



307 records were isolated by sequentially determining the variance left in the trace element records
308 after each of the data treatment steps explained above (see example in **S7**). This procedure
309 allowed us to quantify the amount of variance in each trace element profile explained by either
310 diurnal or semi-diurnal variability.



311 **3. Results**

312 3.1 Trace element data

313 LA-ICP-MS line scans yielded profiles of Sr/Ca, Mg/Ca, Mn/Ca and Ba/Ca in growth direction on
314 11 cross sections through shells of *P. maximus*, *T. maxima*, *T. squamosa* and *T. squamosina*.
315 Trace element profiles of consecutive line scans on the same transect show high repeatability:
316 sub-millimeter scale patterns in Sr/Ca, Mg/Ca, Mn/Ca, and Ba/Ca are repeated between
317 consecutive line scans, R^2 values between trace element results of time-equivalent shell samples
318 typically exceed 0.8, and the mean ratio difference between time equivalent samples in different
319 line scans is less than 0.05 mmol/mol for the most variable profiles (Mg/Ca, with lower differences
320 for the lower-concentration Mn/Ca and Ba/Ca records; see **S2**). Remeasured transects further
321 away from the outer shell surface in tridacnids (see **section 2.4**) differ more from the original
322 transects than those measured on the exact same locality in the shell: R^2 values between parallel
323 lines in different localities are 0.3 – 0.5 for Mg/Ca and Sr/Ca and <0.3 for Mn/Ca and Ba/Ca,
324 reflecting intra-shell variability in trace element composition in the tridacnids (**S2**). Overall, sub-
325 millimeter scale patterns in trace element composition are reproduced in parallel line scans, and
326 the mean offset between the lines was always less than 0.2 mmol/mol.

327 Pectinid and tridacnid shells contain similar mean Sr/Ca and Ba/Ca ratios (Sr/Ca of 1.3 ± 0.3 and
328 1.5 ± 0.6 mmol/mol respectively; Ba/Ca of 2.8 ± 2.5 and 3.0 ± 5.1 $\mu\text{mol/mol}$ respectively;
329 uncertainty is calculated as 1σ). Mean Mg/Ca and Mn/Ca ratios are higher in *P. maximus* than in
330 *Tridacna* species (Mg/Ca = 3.1 ± 0.9 and 0.7 ± 0.9 mmol/mol; Mn/Ca = 7.8 ± 4.7 and 2.7 ± 7.8
331 $\mu\text{mol/mol}$; 1σ ; **Figure 2**; **S4**). Differences between tridacnid specimens generally exceed the
332 differences between tridacnids and pectinids (1σ of Ba/Ca among all tridacnid specimens = 2.1
333 $\mu\text{mol/mol}$). Individual records like those in **TM84** and **PM3_1** show large variability (especially in
334 Ba/Ca and Mn/Ca) compared to other specimens of the same species. Inter-specimen variability
335 is higher in tridacnid shells than in pectinids (inter-specimen relative standard deviations as a

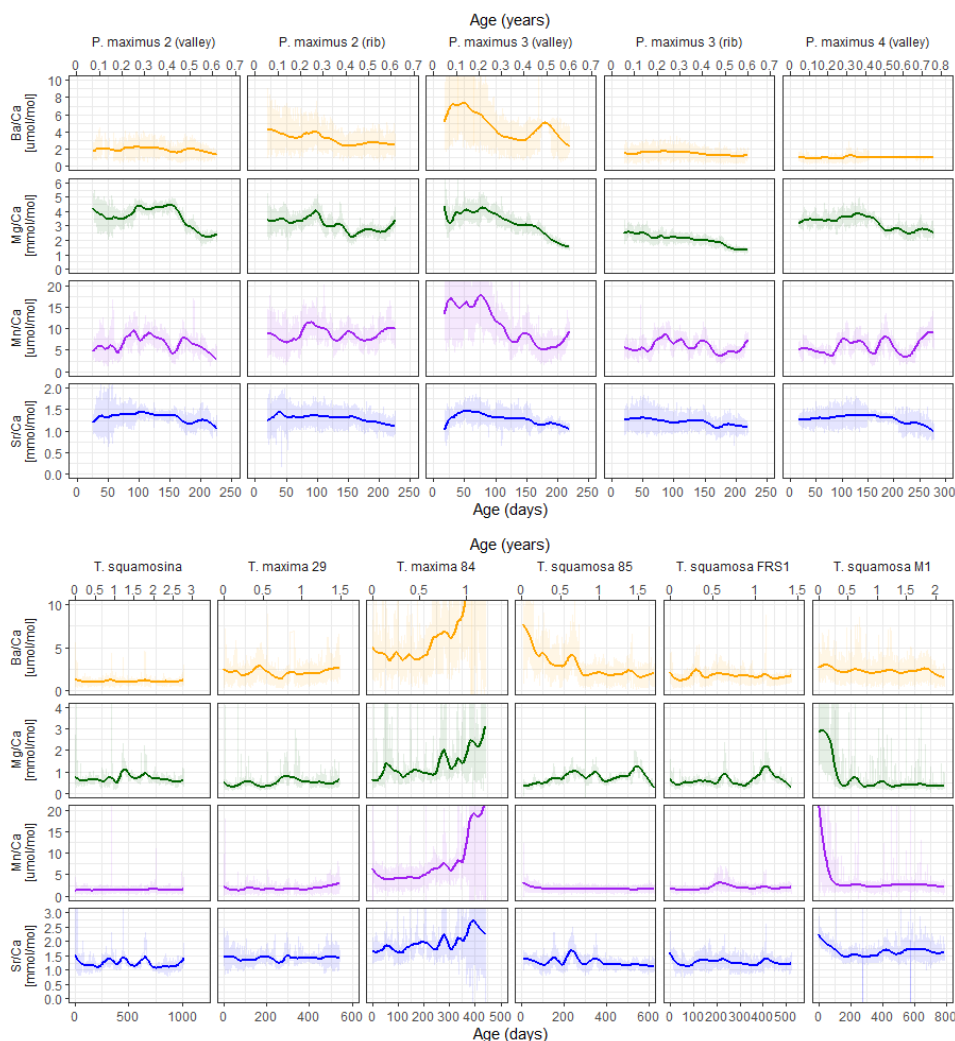


336 fraction of mean ratio for Ba/Ca: 0.74 vs 0.64, Mg/Ca: 0.37 vs 0.20, Sr/Ca: 0.19 vs 0.03 and
337 Mn/Ca: 0.78 vs 0.33 for tridacnids and pectinids, respectively). **Figure 2** shows that this variability
338 between tridacnids is not readily explained by differences between species, but mostly reflects
339 differences in the trends within the records, with some specimens (e.g., **TM84**, **TSM1** and **TS85**)
340 showing trends in composition towards the end of the record (see also **S8**). Trace element
341 compositions in tridacnid shells are significantly more skewed towards higher values than in
342 pectinids (mean skewness per element and per specimen is 9.7 for tridacnids and 0.9 for
343 pectinids), reflecting the high peaks in trace element composition observed in tridacnid profiles,
344 especially near the ventral margin (e.g., specimens **TM84**, **TSM1** and **TS85**; see **section 2.4**; **Fig.**
345 **2**; **S8**). Finally, “rib” and “valley” segments through the same specimen of *P. maximus* show similar
346 patterns in trace elements, but absolute concentrations (especially of Ba and Mn) can be quite
347 different, highlighting heterogeneity within the shells of *P. maximus* (**Fig. 2**).

348 Plots of trace element variability reveal dominant high-frequency variability superimposed on
349 seasonal-scale patterns (**Figure 2**). Trace element profiles in pectinids, reflecting only one
350 growing season, show a typical seasonal pattern in Sr/Ca and Mg/Ca with maxima in the
351 elemental ratio in the middle of the profile (corresponding to the summer). Mn/Ca and Ba/Ca in
352 pectinids are more variable, showing multiple peaks in the same growth year. Peaks in Mn/Ca
353 and Ba/Ca are synchronous between profiles through the same specimen, but not between
354 specimens, possibly showing that growth resumed on different days for different specimens after
355 the winter stop. Like in the pectinid profiles, Mg/Ca, and Sr/Ca ratios in tridacnids show similar
356 patterns, with one or two distinct cycles per growth year. However, higher frequency variability in
357 tridacnid ratio profiles is characterized by more extreme peaks, especially in Mg/Ca, skewing the
358 distribution of trace element values. Mn/Ca and Ba/Ca appear to be less variable in tridacnid
359 shells than in pectinids, except for specimen **TM84**, which shows a sharp increase in Mn and Ba
360 towards the end of its lifetime. Mn/Ca and Ba/Ca ratios in tridacnids show more regular annual or



361 biannual variability than pectinids (most notably specimen **SQSA1**). It must be noted, however,
362 that *P. maximus* shells only recorded one growth season, limiting the interpretation of seasonal
363 growth patterns.



364

365 **Figure 2:** Overview of LA-ICP-MS results of Sr/Ca (blue), Mg/Ca (green), Mn/Ca (purple) and
 366 Ba/Ca (orange) in pectinid (upper panel) and tridacnid (lower panel) specimens. Vertical axes are
 367 equal for plots positioned next to each other (but different for the two groups of tridacnid and
 368 pectinid plots). Shaded lines show raw LA-ICP-MS data while solid lines indicate 0.2 span LOESS
 369 fits through the data highlighting monthly-scale variability. A direct comparison of trace elemental
 370 ratios between specimens is provided in **S8**.



371 3.2 Age models

372 Growth line counting in the *P. maximus* shells was repeated multiple times on both the outer shell
373 surface and in cross sections through the shell by different persons (**Table 1; S3**). The variability
374 in counting results shows that the growth lines were not always equally easy to distinguish. In
375 **PM2** and **PM3**, the most likely number of increments (228 and 220 respectively) was counted in
376 both cross sections and on the outside of the shell, with other analyses yielding both higher and
377 lower numbers. In **PM4**, counts on the outside and on the one available cross section were very
378 close (**Table 1**). In this case, the counting in the cross section (278 increments) was chosen as
379 reference since the LA-ICP-MS profile was measured on the same cross section and could be
380 directly linked to the counted increments. The fact that the mean increment width between the *P.*
381 *maximus* specimens which grew in the same year in the same environment is highly consistent
382 lends confidence to the layer counting result (**Table 1**). The difference in number of days of growth
383 between specimens can be caused either by variability in the day on which seasonal growth
384 commenced (in spring) or the day on which the winter growth stop commenced (in autumn;
385 Chauvaud et al., 1998). The sampling date (November 15th, 2019) does not preclude the onset of
386 winter growth cessation before the time of sampling. The age-distance relationships (growth
387 curves) resulting from the sclerochronology are shown in **S5**.

388



389 **Table 1: Growth increments counting in *P. maximus***

Specimen	Increments counted on outer surface	Increments counted in cross sections	Mean increment width [$\mu\text{m} \pm 1\sigma$]
PM2	226, 228 , 234, 241	227, 228 , 233	249 \pm 19
PM3	220 , 226, 243	213, 220 , 220	249 \pm 22
PM4	272, 273	278	247 \pm 4

390

391



392 Layer counting in tridacnid shells yielded estimates of semi-diurnal, daily and annual growth
393 (**Table 2; S4**). Annual growth rates calculated from layer counting are highly consistent between
394 specimens from the same species from the same environment, lending confidence to the growth
395 line counting results. The von Bertalanffy growth models based on these growth line countings
396 are plotted in **S5**. Statistics of the parameters (L_{inf} and k) of these growth models and their
397 uncertainty are provided in **S4**.

398



399 **Table 2: Growth line counting in *Tridacna* shells.** Column 3 shows the total number of
 400 increments counted in the specimen, column 4 shows their median width and column 5 shows
 401 the width of an annual increment in the specimen. Note that increments could not be counted over
 402 the entire growth period of the shells, so the numbers in column 3 represent representative
 403 numbers of increments counted in those parts of the shells where they were distinct enough for
 404 counting (see **section 2.5**) Increment timing (semi-diurnal vs diurnal) was established based on
 405 the relative difference between small increment width and annual increment width.

Specimen	Species	# counted increments	Median increment width [μm]	Annual growth [mm]	Increment timing
TM29	<i>T. maxima</i>	274	26.5	27.9	Semi-diurnal
TM84	<i>T. maxima</i>	109	39.1	26.6	Diurnal
TS85	<i>T. squamosa</i>	310	40.3	20.2	Diurnal
TSFRS1	<i>T. squamosa</i>	225	23.3	20.1	Semi-diurnal
TSM1	<i>T. squamosa</i>	180	33.3	20.6	Diurnal
SQSA1	<i>T. squamosina</i>	153	22.3	14.9	Diurnal

406

407



408 Growth rates are highly similar between specimens of the same species (**Table 1 and Table 2;**
409 **S3-5**), with *P. maximus* achieving the highest growth rates (~ 220 growth days * ~ 250 $\mu\text{m}/\text{d} \approx 55$
410 mm/yr ; **Table 1**), followed by *T. maxima* (~ 27 mm/yr ; **Table 2**), *T. squamosa* (~ 20 mm/yr ; **Table**
411 **2**) and *T. squamosina* (15 mm/yr ; **Table 2**). The age models reveal that the average temporal
412 resolution of the LA-ICP-MS line scans was 0.04h, 0.24h, 0.44h and 0.27h for *P. maximus*, *T.*
413 *maxima*, *T. squamosa* and *T. squamosina*, respectively. These estimates were calculated by
414 dividing the width of the daily increments (e.g., 250 μm for *P. maximus*) by the resolution of the
415 LAICPMS data (0.4 μm) to obtain the number of LAICPMS measurements per day (e.g., 625
416 pts/day for *P. maximus*, yielding a mean sampling resolution of 0.04h). Note that the LA-ICP-MS
417 slit is wider (20 μm) than the spatial sample resolution, causing some smoothing on the scale of
418 this very fine temporal resolution. The LA-ICP-MS profiles record trace element variability during
419 growth periods ranging between 220 days (for **PM3**) and 1041 days (for **SQSA1**).

420

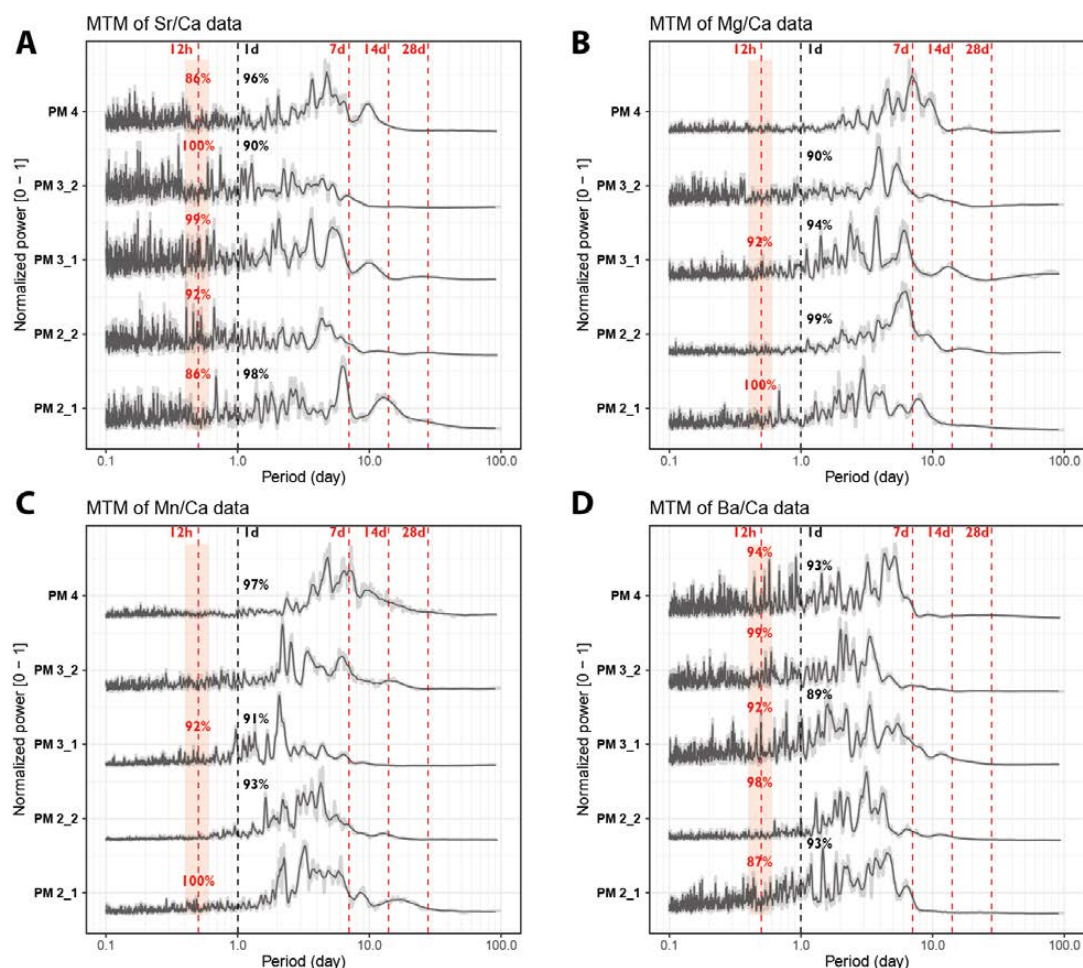
421 3.3 Spectral analysis

422 Normalized power spectra and significance level of daily and tidal periodicities in pectinid and
423 tridacnid records are shown in **Figure 3** and **Figure 4**, respectively. Full spectral analysis results
424 for all trace element records in all specimens are provided in **S9**. All *P. maximus* power spectra
425 (**Fig. 3**) reveal semi-diurnal (12h) periodicity in Sr/Ca and Ba/Ca with $>86\%$ statistical significance.
426 Only sections through the ribs of the shells (**PM2_1** and **PM3_1**) show semi-diurnal periodicity in
427 Mg/Ca and Mn/Ca ($>90\%$ significance). Daily periodicity is present in some pectinid profiles, but
428 there seems to be no consistent pattern in the presence of diurnal variability between specimens,
429 between sections through ribs or valleys in the shell or between trace element records. Most
430 power spectra of trace element profiles in pectinids show peaks associated with multi-day tidal
431 periodicities, the most dominant being a 7-day period, with weaker expression of cyclicity
432 associated with the fortnightly (14d) cycle or lunar month (28d). The latter is partly suppressed by



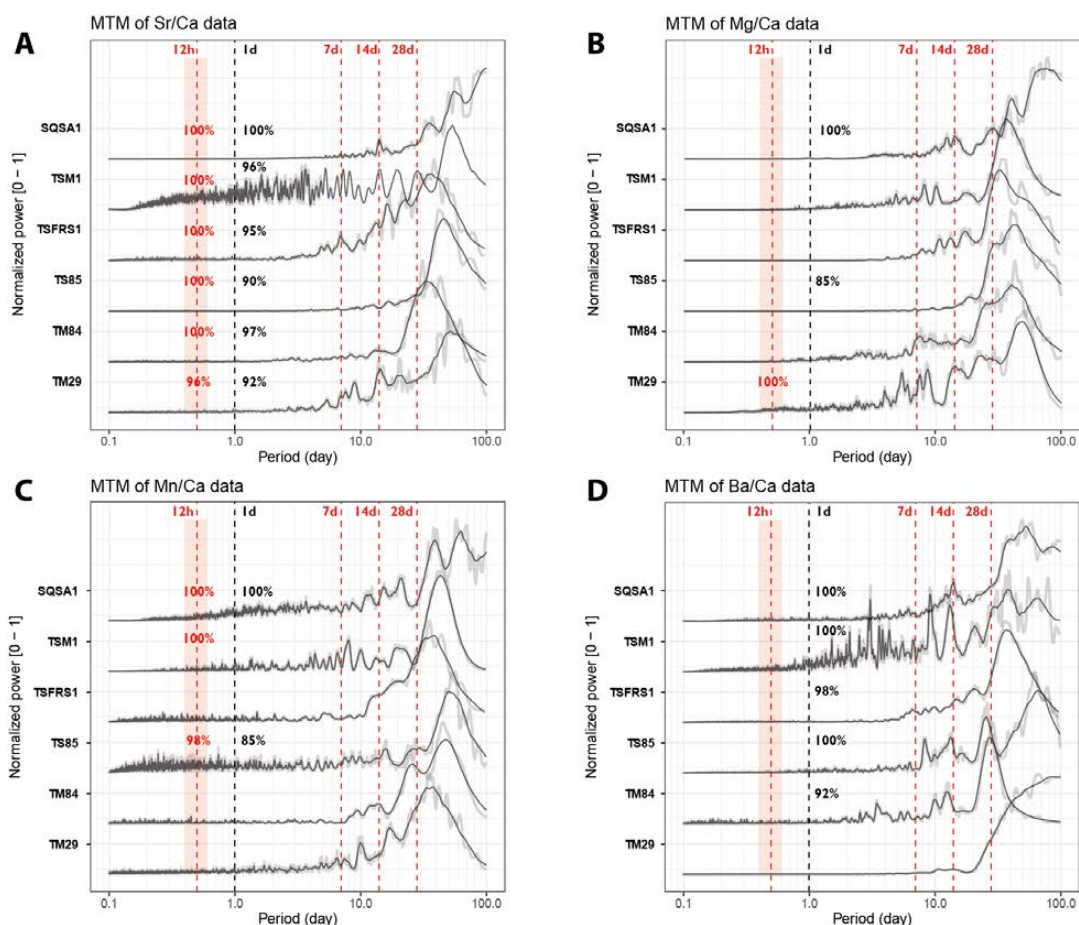
433 the 0.2 span LOESS filter (equivalent to a 44-56 day period depending on the length of the record)
434 applied on the records to remove the seasonal trend from the records. However, these lower
435 frequency cycles are clearly visible in the wavelets (see **S9**).

436 A much more consistent expression of diurnal periodicity is found in the tridacnid trace element
437 profiles compared to those in the pectinids (**Fig. 4**). Especially Sr/Ca and Ba/Ca records through
438 nearly all tridacnid specimens exhibit strong (>90% confidence level) power in the daily period,
439 while Mn/Ca and Mg/Ca records exhibit much less periodicity. Sr/Ca records in the tridacnids also
440 contain a significant (>96%) semi-diurnal component, whose tidal origin seems clear in most
441 specimens by peaks in power in the longer (7d, 14d and 28d) tidal components.



442

443 **Figure 3:** Multi-taper method spectrograms of Sr/Ca (A), Mg/Ca (B), Mn/Ca (C) and Ba/Ca (D)
 444 records through the five pectinid cross sections after detrending (see **section 2.6**). All spectra are
 445 normalized by dividing by the highest power peak and plotted on the same horizontal axis. Grey
 446 shaded lines show raw data while solid black lines plot 21-point moving average smoothed
 447 curves. Red vertical dashed lines highlight the expected periods of tidal variability while black
 448 vertical dashed lines indicate 1-day periodicities. Significance levels of peaks on these periods
 449 (see **section 2.6** and Meyers, 2012) are rounded to the nearest whole percentage point.



450

451 **Figure 4:** Multi-taper method spectrograms of Sr/Ca (A), Mg/Ca (B), Mn/Ca (C) and Ba/Ca (D)
 452 records through the six tridacnid cross sections after detrending (see **section 2.6**). All spectra are
 453 normalized by dividing by the highest power peak and plotted on the same horizontal axis. Grey
 454 shaded lines show raw data while solid black lines plot 21-point moving average smoothed
 455 curves. Red vertical dashed lines highlight the expected periods of tidal variability while black
 456 vertical dashed lines indicate 1-day periodicities. Significance levels of peaks on these periods
 457 (see **section 2.6** and Meyers, 2012) are rounded to the nearest whole percentage point.

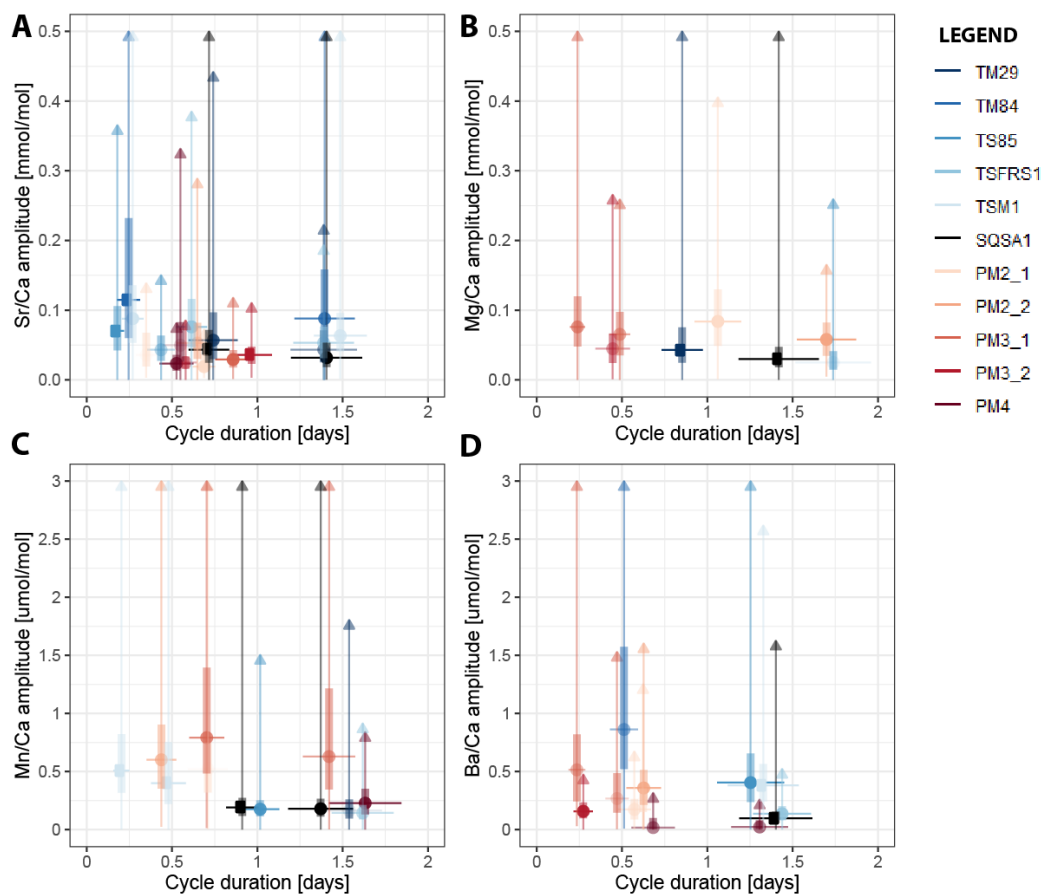
458



459 3.4 Variance decomposition

460 Variability at the daily (24h) and tidal (12h) scale in all trace element records through all specimens
461 was extracted using bandpass filtering (**section 2.7**; see **S9** and **S10**). The median amplitude of
462 variability within these stacks was plotted against the median period of the variability per element
463 and per specimen to highlight dominant periodicities in the trace element data (**Figure 5**). As
464 noted in the spectral analysis results (**section 3.3**), trace element composition in tridacnid shells
465 is more strongly controlled by daily variability than in pectinid shells (**Fig. 5**; **S10**). The difference
466 is especially noticeable in Sr/Ca and Ba/Ca ratios, which show a clear divide between daily
467 periodicity in tridacnid shells and tidal periodicity in pectinids (see **Fig. 5**). The differences in
468 Mg/Ca and Mn/Ca ratios are less clear.

469



470

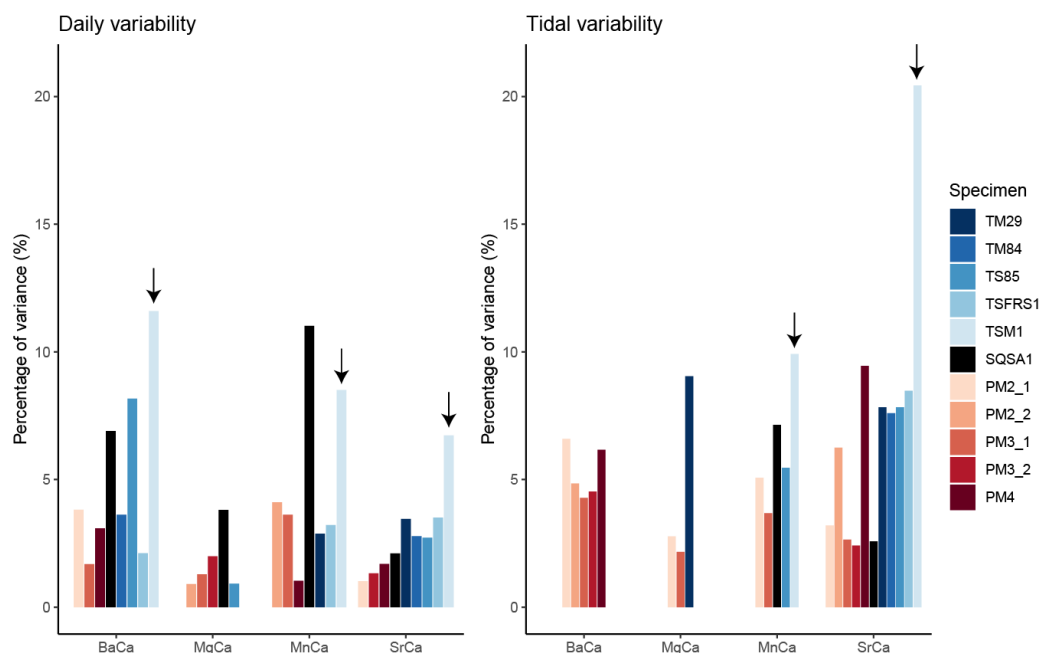
471 **Figure 5:** Cross plot showing the amplitude of variability of dominant spectral periods in Sr/Ca
 472 (A), Mg/Ca (B), Mn/Ca (C) and Ba/Ca (D) against the period (duration) of the cycle. Round
 473 symbols indicate the median amplitude of the cycle, while vertical bars and lines show interquartile
 474 differences and ranges in the amplitude over the record. Horizontal bars indicate the width of the
 475 bandpass filter used to extract periodic variability. Colors highlight different specimens (see
 476 legend).

477



478 An example of the distribution of normalized variability within the trace element records after each
479 data processing step is shown in **S7**. From this example it is clear that a large fraction of the
480 variance in the records (73% in this record after trimming outliers) is explained by low-frequency
481 variability (**S7**). Of the remaining smoothed and detrended dataset, at most 20% of the variance
482 is explained by daily and tidal (semi-diurnal) periodicity (see **Figure 6** and **Table 3**). A full
483 decomposition of variance in all trace element records through all specimens is provided in **S7**.
484 **Figure 5** and **Figure 6A** shows that, overall, the variance explained by daily periodicity is higher
485 in tridacnids than in pectinids (Wilcoxon signed rank test; $W = 44$; $p = 0.009$). The difference
486 between species is smaller for tidal variability (**Fig. 6B**). There is no clear difference in relative
487 dominance of tidal variability between trace element records, but daily variability is more strongly
488 expressed in Ba/Ca and Mn/Ca records, especially in tridacnid shells. Finally, *T. squamosa*
489 specimen **TSM1**, which grew under a sunshade, does not exhibit significantly lower daily
490 periodicity compared to the other tridacnid specimens.

491



492

493 **Figure 6:** Summary of relative variance (in %) of significant daily (left) and tidal (right) variability
494 extracted from trace element records. Colors highlight different specimens (see legend). Note that
495 the *T. squamosa* specimen **TSM1** which grew under a sunshade is highlighted with a black arrow.

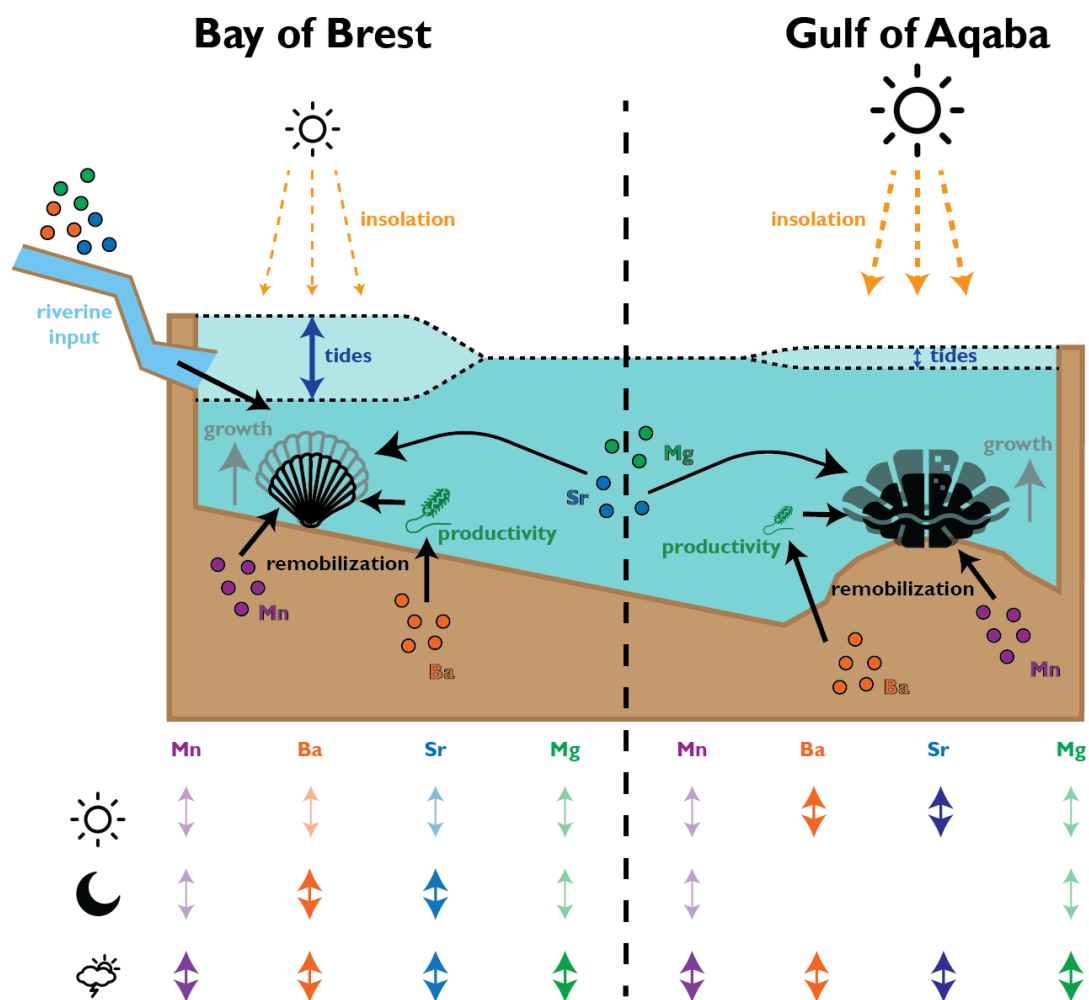
496



497 **Table 3:** Overview of the relative (in %) variance associated with daily and tidal variability in all
 498 trace element records through all specimens. Empty cells represent records for which no
 499 significant tidal or daily periodicity was found (see Fig. 3-4).

	Daily variance				Tidal variance			
	[% relative to detrended record]				[% relative to detrended record]			
	Ba/Ca	Mg/Ca	Mn/Ca	Sr/Ca	Ba/Ca	Mg/Ca	Mn/Ca	Sr/Ca
PM2_1	3.8 %			1.0 %	6.6 %	2.8 %	5.1 %	3.2 %
PM2_2		0.9 %	4.1 %		4.9 %			6.3 %
PM3_1	1.7 %	1.3 %	3.6 %		4.3 %	2.2 %	3.7 %	2.7 %
PM3_2		2.0 %		1.3 %	4.5 %			2.4 %
PM4	3.1 %		1.0 %	1.7 %	6.2 %			9.5 %
TM29			2.9 %	3.5 %		9.0 %		7.8 %
TM84	3.6 %			2.8 %				7.6 %
TS85	8.1 %	0.9 %		2.7 %			5.5 %	7.8 %
TSFRS1	2.1 %		3.2 %	3.5 %				8.5 %
TSM1	12 %		8.5 %	6.7 %			10 %	20 %
SQSA1	6.9 %	3.8 %	11 %	2.1 %			7.1 %	2.6 %

500



501

502 **Figure 7:** Schematic overview of environmental parameters interpreted to affect shell growth and
 503 composition of pectinids in the Bay of Brest and tridacnids in the Gulf of Aqaba. The table at the
 504 bottom provides a schematic qualitative overview of the amount of variance in the trace element
 505 records of the taxa is explained by daily (sun symbol), tidal (moon symbol) or aperiodic (cloud
 506 symbol) variability in the environment.

507



508 **4. Discussion**

509 4.1 Trace element variability in *P. maximus*

510 4.1.1 Comparison with previous studies

511 Trace element concentrations in *P. Maximus* analyzed in this study are in close agreement with
512 concentrations found in wild (live collected) *pectinid* shells in the literature (Lorrain et al., 2005;
513 Barats et al., 2008; Poitevin et al., 2020; Fröhlich et al., 2022). In these studies, Sr/Ca shows a
514 strong link with calcification rate (as measured by the width of daily shell increments; Lorrain et
515 al., 2005), although previous studies did not assess variability on the (sub-)daily scale. The long-
516 term trends in our Sr/Ca records seem to confirm this correlation, with higher values being
517 recorded in the middle of the growing season (day 50-150; **Fig. 2**) when growth rates are highest
518 (see **S5**). There is some discussion on the dependence of Mg/Ca ratios in pectinid shells to
519 temperature and/or salinity (Lorrain et al., 2005; Poitevin et al., 2020). This study's individuals that
520 grew during the same year in the same environment do not show a synchronous Mg/Ca pattern
521 (**Fig. 2**), arguing against a simple temperature dependence for Mg/Ca in *P. maximus*. In addition,
522 the lack of strict coherence between profiles of Mg/Ca (and other elements) in parallel transects
523 through *P. maximus* shells (e.g., **PM2_1** and **PM2_2**; **Fig. 2**) hints at compositional heterogeneity
524 within the shells. Low correlations between profiles through the same shell at the daily scale are
525 also partly driven by small misalignments of the timing of shell formation between the transects
526 at the sub-millimeter scale and variations in the height of trace element peaks, especially in Mn/Ca
527 and Ba/Ca, which are higher further towards the outside of the shell (**S2**). There is evidence
528 suggesting that Mg content varies in mollusk shells in function of the amount of organic matter in
529 the biomineral (Dauphin et al., 2003; Richard, 2009; Tanaka et al., 2019). Contrarily, Mn is taken
530 up in thermodynamic equilibrium in the mineral fraction of bivalve shells (Onuma et al., 1979;
531 Soldati et al., 2016), and Mn/Ca ratios in *P. maximus* have been shown to faithfully record
532 fluctuations of dissolved Mn in the coastal environment driven by riverine input and redox



533 conditions (Barats et al., 2008). Similarly, there is strong evidence that Ba/Ca ratios in *P. maximus*
534 (and other mollusks) record changes in Ba available in the environment linked to primary
535 productivity (e.g., Gillikin et al., 2008; Thébault et al., 2009; Fröhlich et al., 2022). This relationship
536 would explain the skewed (skewness > 1; **S8**) character of the Ba/Ca records and the correlation
537 between Ba/Ca and Mn/Ca in our *P. maximus* specimens, as the reducing conditions following
538 peaks in primary productivity favor the remobilization of Mn into the water column causing short-
539 lived simultaneous increases in Ba/Ca and Mn/Ca in the shells (Dehairs et al., 1989; Barats et al.,
540 2008; 2009).

541 4.1.2 Short-term changes in shell composition in tridacnids

542 In the context of the high-resolution trace element variability central to this study, it seems
543 plausible that short-term changes in the environment of the Bay of Brest were drivers of Mn/Ca
544 and Ba/Ca variability in *P. maximus* shells, while Mg/Ca and Sr/Ca composition is mostly driven
545 by changes in calcification rate. This would suggest that the significant tidal (12h) component in
546 Ba/Ca and Mn/Ca records through *P. maximus* (**Fig. 3**) is driven directly by redox changes over
547 the strong tidal cycle in the Bay of Brest (see Polsenaere et al., 2021) and resuspension of Ba
548 and Mn due to tidal currents (Hily et al., 1992), while tidal rhythms in Mg/Ca and Sr/Ca may be a
549 consequence of the scallop's calcification response to changes in its environment (e.g.,
550 temperature, salinity and light availability) through the large (up to 7m range) tidal cycle (**Fig. 7**).
551 The latter corroborates with previous studies in other calcitic mollusk shells which demonstrated
552 that Mg incorporation on short timescales is driven by the metabolic response to subtle changes
553 in the environment (Lazareth et al., 2007). Finally, care must be taken to interpret trace element
554 variability in *P. maximus* shells, since large intra-shell gradients in Mg/Ca, Sr/Ca and Mn/Ca have
555 previously been observed in this species, making trace element composition highly dependent on
556 the location of measurements relative to the outer shell surface or positioning relative to striae on
557 the shell surface (Freitas et al., 2009). Even though the LA-ICP-MS line scans in this study



558 targeted exclusively the oOSL of *P. maximus* specimens, variability in elemental ratios resulting
559 from small changes in the distance of the line scan from the outer edge of the shell cannot be fully
560 excluded (Richard, 2009).

561

562 4.2 Trace element variability in tridacnids

563 4.2.1 Comparison with previous studies

564 Results for Sr/Ca, Mg/Ca and Ba/Ca in this study's tridacnid specimens broadly corroborate trace
565 element results in other tridacnid studies (e.g., Elliot et al., 2009; Sano et al., 2012; Yan et al.,
566 2013; Warter et al., 2018). While data on Mn/Ca in the OSL of tridacnids is scarce, the Mn/Ca
567 ratios in tridacnids in this study (mean Mn/Ca = 7.8 ± 4.7 $\mu\text{mol/mol}$) are similar to LAICPMS Mn/Ca
568 data available in the literature (Warter et al., 2015, 4-10 $\mu\text{mol/mol}$), but significantly lower than
569 Mn/Ca values measured using total digestion Atomic Absorption Spectrometry (Madkour, 2005,
570 ~ 30 $\mu\text{mol/mol}$). The main difference between the techniques is that LA-ICP-MS (both in this study
571 as in Warter et al., 2015) sampled shell layers where growth lines were visible and did not include
572 pre-treatment, while the total digestion study (Madkour, 2005) removed organic matter by roasting
573 the shells at 200°C prior to bulk shell analysis. The difference in results may therefore hint at
574 differences between shell layers within tridacnids, or differences in Mn concentration between the
575 organic and mineral fractions in the shells. Bivalve typically contain between 1% and 5% organic
576 matter (Marin and Luquet, 2004), with tridacnid shells being notable for their low organic matter
577 content (<1%; Agbaje et al., 2017; Taylor and Layman, 1972). Given that most Mn in bivalve
578 shells is typically associate with the mineral fraction of the shell (Soldati et al., 2016), it seems
579 unlikely that such a large fraction of Mn could originate from the organic matrix. Therefore, we
580 consider a difference in Mn concentration between shell layers in tridacnids more likely. The lack
581 of consistent trace element offsets between the tridacnid species under study here (*T. maxima*,



582 *T. squamosa* and *T. squamosina*) confirms the chemical similarities of shells tridacnid species
583 found in previous studies (e.g., *T. gigas*; Elliot et al., 2009; Yan et al., 2013; *T. crocea*; Warter et
584 al., 2018; *T. derasa*; Sano et al., 2012).

585 4.2.2 Short-term variability in Sr/Ca

586 Sr/Ca in tridacnids is thought to be strongly controlled by light intensity through a circadian rhythm
587 linked to the day-night cycle (Sano et al., 2012; Warter et al., 2018). This would explain the strong
588 daily periodicity in Sr/Ca records through all tridacnids in this study. This daily periodicity may be
589 caused by the ctenidium in tridacnids working on a daily rhythm to keep the acid-base balance in
590 the hemolymph of the clams to offset the CO₂ depletion by photosymbionts (which is paced to the
591 day-night cycle of light availability). In the process, Ca²⁺-channels and Na⁺/H⁺-exchangers work
592 to keep the charge balance in the internal fluid and provide nutrients and ions for shell
593 mineralization, letting in compatible trace elements such as Sr²⁺ (Ip and Chew, 2021). This
594 mechanism could explain the indirect link between trace element uptake in the shell in tridacnids
595 and the day-night cycle without a direct causal relationship between trace element concentration
596 and light availability (as demonstrated by the strong daily cycle in trace elements in the shaded
597 **TSM1** specimen). It is worth noting that experiments on freshwater bivalves (e.g., *Corbicula*
598 *fluminea*; Zhao et al., 2017) revealed that a closure of the Ca²⁺ channels did not influence Sr
599 concentrations in the shell, arguing against a kinetic effect on Sr partitioning into the shell.

600 4.2.3 Tidal vs. diurnal variability

601 Our spectral analysis does not allow us to distinguish between the expression of the solar day
602 (24h) and lunar day (~24.8h) because the width of the bandpass filters used to extract periodicities
603 encompass both frequencies. While we cannot exclude the possibility that some of the daily (24h
604 frequency band) periodicity in tridacnid records is an expression of the lunar cycle, it seems
605 unlikely for most records except Sr/Ca, because the expression of the other lunar cycles (most



606 notably the ~12h cycle) is much weaker in tridacnids compared to the pectinids. Nevertheless, it
607 remains possible that the diurnal cycle in Sr/Ca in tridacnids, previously interpreted as a response
608 to the day-night cycle, is in fact caused by a circadian rhythm paced to the lunar day. Additionally,
609 vertical mixing, a major driver of sea surface temperature changes in the northern Gulf of Aqaba
610 is shown to be driven by a combination of surface wind intensity (which has strong daily variability)
611 and the presence of tidal currents (Carlson et al., 2014). It is therefore possible that changes in
612 local surface water temperature partly control the observed (semi-)diurnal variability.

613 4.2.4 Seasonal variability

614 On longer (seasonal) timescales, Sr/Ca in tridacnids has been suggested as a temperature proxy
615 similar to the well-known Sr/Ca-Sea Surface Temperature relationship in tropical corals (Lough,
616 2010; Yan et al., 2013). However, significantly lower Sr/Ca ratios in tridacnids compared to coral
617 aragonite (1.5 – 2.0 mmol/mol vs. 7.5 – 9.5 mmol/mol in corals; Elliot et al., 2009; **Fig. 2**) suggest
618 that tridacnids exert a large degree of biological control on the Sr concentration in their shells,
619 either possibly through the light-sensitive photosymbiosis-calcification relationship outlined above
620 or otherwise through active Sr removal from the biomineralization site by Sr-binding organic
621 molecules. Similarly, Mg/Ca ratios in tridacnids were previously thought to primarily record water
622 temperature (e.g., Batenburg et al., 2011) but detailed investigation shows here large differences
623 in Mg concentration within tridacnid shells. and a strong anticorrelation of Mg with sulfur
624 compounds associated with the organic matrix in the shell (see **section 4.1**; Dauphin et al., 2003),
625 has been put forward as evidence for a strong control of calcification and microstructure on Mg
626 composition in tridacnid shells (Yoshimura et al., 2014). However, evidence from studies on
627 foraminifera calcification demonstrate that the sulfur in biocarbonates is not organically bound
628 and that the covariation with Mg might instead be caused by lattice distortion due to incorporation
629 of Mg favoring simultaneous S incorporation (van Dijk et al., 2017).

630 4.2.5 Ba/Ca and Mn/Ca in tridacnids



631 As in the pectinids, Ba/Ca ratios in tridacnids likely reflect changes in Ba in the environment, which
632 can be caused by river input, upwelling of comparatively nutrient-rich waters or blooms of Ba-rich
633 phytoplankton (Vander Putten et al., 2000; Elliot et al., 2009). Given that Mn is mostly associated
634 with the mineral fraction of bivalve shells and seems to fractionate into the shell close to
635 equilibrium with seawater (Onuma et al., 1979; Soldati et al., 2016), Mn/Ca ratios in tridacnids
636 likely reflect the availability of dissolved Mn in the water column, as in other mollusk taxa (e.g.,
637 Barats et al., 2008; see **section 4.1**). This assumption is supported by the correlation between
638 Mn/Ca and Ba/Ca measured in this study (**Fig. 2**), suggesting that both records are influenced on
639 seasonal timescales by variability in nutrient availability and redox conditions (*sensu* Dehairs et
640 al., 1989). Part of this correlation between Mn/Ca and Ba/Ca is driven by synchronous increases
641 in both elements near the start and end of the profiles through tridacnid shells (**Fig. 2**). These
642 changes may reflect a decrease of control on shell composition during periods of stress, or
643 alternatively reflect periods of slower growth which cause more primitive microstructures
644 (characterized by higher concentrations of trace elements) to be formed (Warter et al., 2018).

645 4.2.6 Environmental changes in the Gulf of Aqaba

646 Given that the Gulf of Aqaba is oligotrophic, seasonally stratified, and lacks significant riverine
647 input (Nassar et al., 2014; Manasrah et al., 2018), the variability in nutrient concentrations and
648 redox conditions driving Mn/Ca and Ba/Ca variability in tridacnids are likely driven by convective
649 overturning. The tidal amplitude is much smaller than in the Bay of Brest (<1 m; Manasrah et al.,
650 2018) and is unlikely to drive significant short-term fluctuations in sea water chemistry. This may
651 therefore explain the lack of tidal (12h) periodicity in Ba/Ca and Mn/Ca in tridacnids (**Fig. 5**).
652 Nevertheless, tidal rhythms have been observed in the behavior and growth of deep-sea bivalves
653 living far below the direct influence of tides on the environment, proving that such patterns can be
654 recorded by the animals through their circadian rhythm (Schöne and Giere, 2005; Nedoncelle et
655 al., 2013; Mat et al., 2020). In this case, the daily cycle seems to have been more important for



656 Ba/Ca in tridacnids, plausibly by driving diurnal changes in primary productivity in the Gulf of
657 Aqaba. Alternatively, the daily periodicity found in tridacnid shell chemistry may in fact be a
658 response to the lunar day (~24.8h) cycle, which is imprinted in the shell's chemical composition
659 through periodic exposure of the clams to extreme heat or air (subaerial exposure) in their shallow
660 water environment during exceptionally low tides. The stress induced from this exposure could
661 have affected calcification and incorporation of trace elements (see above).

662 Interestingly, Sr/Ca ratios in tridacnids do exhibit tidal periodicity (**Table 2**), perhaps driven by a
663 circadian rhythm in calcification linked to the tidal cycle, or by subtle changes in water temperature
664 driven by tidal currents (Carlson et al., 2014). This 12h periodic behavior is not observed in
665 previous studies of Sr/Ca ratios in tridacnids (Sano et al., 2012; Warter et al., 2018). A recent
666 valvometric study on tridacnids found a 12h period in activity, which supports the hypothesis that
667 a circadian rhythm paced to the tidal cycle could influence shell calcification (Killam et al., 2022).
668 Significant daily fluctuations in solar radiation (up to 1500 W m⁻²; Manasrah et al., 2018) likely
669 exerted a dominant control on the calcification of tridacnids, explaining the strong diurnal
670 periodicity in Sr/Ca and Ba/Ca records in this study (see **Fig. 7** and **Fig. 9**). As in the (non-
671 symbiotic) pectinid data, it seems likely that the majority of Mn/Ca and Ba/Ca variability in
672 tridacnids directly reflects changes in the chemistry of the sea water and its constituents (e.g.,
673 particulate organic matter) while Mg/Ca and Sr/Ca variations are driven by changes in calcification
674 and microstructure. The latter may be indirectly influenced by light intensity through
675 photosynthesis by the symbionts, or by circadian rhythms paces to the diurnal or tidal cycle.

676

677 4.3 Role of photosymbiosis on high-frequency chemical variability

678 4.3.1 Effect of symbiosis on calcification



679 While the amplitude of diurnal variability in trace element concentrations does not vary much
680 between the symbiotic tridacnids and the non-symbiotic pectinids (**Fig. 5**), the amount of variance
681 in the trace element records explained by daily cyclicity is up to twice as high in tridacnids (**Fig.**
682 **6; Table 3**). This suggests that the 24h cycle has a much larger relative influence on trace element
683 composition (especially Sr/Ca and Ba/Ca) in tridacnids than in pectinids. This seems to point
684 towards a role of the photosymbionts in calcification by tridacnids, such as through symbiont-
685 mediated diurnal variation in the pH of the extrapallial fluid (Ip et al., 2006), as well as active
686 transport of HCO_3^- for calcification (Chew et al., 2019) and as a C supply to the symbionts from
687 the host (Boo et al., 2021). Given the differences in absolute ratios between these two groups of
688 bivalves, comparing variance yields a more robust assessment of the relative importance of tidal
689 or diurnal variability on shell composition than looking at the absolute size (amplitude) of the
690 chemical cycle. While the difference in variance is clear, the importance of diurnal cyclicity on the
691 photosymbiotic tridacnids is not as big as one might expect. Rarely more than 10% of the variance
692 is explained by day-night variability (**Table 3**). This seems to contradict the large daily Sr/Ca
693 amplitudes found in Warter et al. (2018) and the trace element fluctuations found in de Winter et
694 al. (2020), which rival the seasonal cycle in these trace element ratios in terms of amplitude.
695 However, the percentages in **Table 3** relate to the amount of variation in the complete records
696 through these individuals and therefore also contain areas of the shell where daily cyclicity is less
697 pronounced, while values in previous studies often reflect maximum amplitudes recorded in parts
698 of the shell with exceptionally clear daily increments.

699 4.3.2 Effect of differences in the environment

700 It seems plausible that part of the difference in diurnal variability between pectinids and tridacnids
701 is explained by a difference in the environment between the Gulf of Aqaba and the Bay of Brest,
702 rather than the presence of photosymbionts. The diurnal insolation cycle in the Gulf of Aqaba is
703 larger than in the Bay of Brest (1500 vs 546 $\text{W}\cdot\text{m}^{-2}$ maximum summer irradiance; Roberts et al.,



704 2018; Manasrah et al., 2019). If calcification in pectinids would be equally sensitive to sunlight,
705 this difference may explain much of the difference between the species. In this scenario, part of
706 the strong tidal component in the pectinid trace element data may be explained by the influence
707 of differences in water depth on the penetration of sunlight through the murky waters of the Bay
708 of Brest (Roberts et al., 2018). In fact, tidal movement can cause strong non-linear amplification
709 or reduction of the solar irradiance at the sea floor of the Bay of Brest by factors exceeding 10,
710 especially outside the summer months, which in turn has a significant effect on primary
711 productivity in the water column (Roberts et al., 2018). This tidal effect is likely to be much weaker
712 in the Gulf of Aqaba, given its comparatively low tidal amplitude, clear oligotrophic waters, and
713 much stronger and less seasonal day-night cycle (Manasrah et al., 2019). Indeed, even in non-
714 photosymbiotic bivalves, light and food availability are demonstrated to be major drivers of the
715 animal's behavior (e.g., Ballesta-Artero et al., 2017). The combination of the daily and tidal cycles
716 on solar irradiance at depth and photosynthesis in the Bay of Brest may therefore pose an
717 alternative pathway for strong tidal cyclicity in the trace element composition of pectinids in this
718 study and account for part of the twofold increase in daily variability in tridacnids compared to the
719 pectinids (**Fig. 6-7; Table 3**).

720 4.3.3 Effect of direct insolation

721 Specimen **TSM1** poses an interesting case study for investigating the link between sunlight and
722 calcification in tridacnids, since it grew under a sunshade and therefore experienced a dampened
723 diurnal variability in insolation compared to other giant clams in the area. The fact that this
724 specimen exhibits similar or even higher diurnal variability in shell chemistry (**Fig. 6**) argues
725 against a direct influence of the rate of photosynthesis itself on calcification. Instead, it seems that
726 daily chemical variability is mostly an expression of circadian rhythm in tridacnids, which is
727 strongly (evolutionarily) coupled to the day-night cycle to optimize the symbiosis with primary
728 producers in its mantle, possibly through respiration rhythms carried out by the ctenidium (see



729 **section 4.2;** Ip and Chew, 2021). Symbionts have been shown to directly aid in calcification in
730 terms of proton pumping (Armstrong et al., 2018), influencing internal acid-base chemistry (Ip et
731 al., 2006), and valvometric studies show the clams bask in sunlight in daylight hours and close
732 partially at night when symbiosis is likely reduced (Schwartzmann et al., 2011). This conclusion
733 is further supported by the lack of a clear difference in diurnal cyclicity between trace element
734 records in *T. maxima*, *T. squamosa* and *T. squamosina* (**Fig. 6; Table 3**), even though the degree
735 of reliance on photosymbiosis is demonstrated to be highly variable between these species
736 (Killam et al., 2020). Therefore, it seems unlikely that sub-daily resolved trace element records in
737 tridacnids can be used as quantitative recorders of paleo-insolation, as was originally suggested
738 by Sano et al. (2012). While the degree of symbiotic activity may not be clearly recorded in the
739 daily amplitude of trace element oscillations, the greater consistency of daily periodic signal in the
740 studied giant clams could relate to the direct biological control exerted by the symbionts on the
741 hosts' rhythms of calcification. Light exposure in giant clams promotes expression of genes coding
742 for proteins involved Ca^{2+} , H^+ and HCO_3^- transport in the mantles of giant clams (Ip et al., 2017;
743 Chew et al., 2019), with the expression proposed to be at least partially mediated by photosensing
744 on the part of the symbionts themselves (Ip et al., 2017). Differences between the daily
745 consistency (spectral power) of photosymbiotic and non-photosymbiotic trace element profiles
746 might still allow paleontologists to use the presence of strong daily periodicity as a proxy for
747 photosymbiosis in the fossil record (as suggested in de Winter et al. 2020). However, the small
748 differences found between pectinids and tridacnids in this study and the comparatively large
749 influence of environmental variability show that such records should be interpreted with caution.
750 Future studies could measure photosynthetic activity of the symbionts in tridacnids and attempt
751 to relate this to the trace element composition of the shell in an attempt to isolate the direct effect
752 of photosymbiosis on shell composition.

753



754 4.4 Aperiodic drivers of shell chemistry

755 4.4.1 Circadian and behavioral changes

756 Even after controlling for instrumental noise, most (~90%) of the variance observed in our trace
757 element records is not directly related to the diurnal or tidal cycle. This suggests that aperiodic
758 events at the scale of hours to days play an important role in the calcification of pectinids and
759 tridacnids. Given the large difference in ecological niche (e.g., photosymbiotic versus non-
760 symbiotic) between these taxa, and the difference between the environment in which they grew,
761 this observation suggests that calcification of bivalves at the (sub-)daily scale may generally be
762 dominated by aperiodic variability in calcification or in the environment. Part of this unaccounted
763 variability may be caused by variability in the animal's behavior, as documented by observations
764 of siphon and valve gape activity in cultured or monitored specimens of a variety of bivalve taxa
765 (Rodland et al., 2006; Ballesta-Artero et al., 2017). While these experiments revealed quasi-
766 periodic (3-7 minute and 60–90 minute periods) behavior unassociated with the tidal or daily cycle,
767 records of activity of the individuals also reveal less regular patterns on the scale of 2-24h which
768 may contribute to the aperiodic variance in trace element records (Rodland et al., 2006). Another
769 example of aperiodic behavior potentially influencing shell chemistry is rapid valve adduction or
770 “coughing” observed in both pectinids and tridacnids, which serves as a mechanism for expelling
771 respiratory CO₂ and faeces from the pallial cavity or to evade predation attempts (Robson et al.,
772 2012; Soo and Todd, 2014). This behavior could resuspend sediment and produce pulses of Mn
773 and Ba at the sediment-water interface which are recorded as short-term, aperiodic variability in
774 these elements in the shell. The temporal sampling resolution (>1h) of trace element records after
775 smoothing out measurement noise does not allow us to resolve periodic variability at the sub-
776 hourly scale cited in these previous studies, meaning that aperiodic variability in behavior and
777 aliasing of these ultradian patterns likely contribute to the aperiodic variability in our trace element
778 records. On longer (sub-)seasonal timescales, activity in bivalves is shown to be highly dependent



779 on food and light availability (Ballesta-Artero et al., 2017), suggesting that aperiodic, short-term
780 changes in these environmental factors could be a main driver of shell growth and composition
781 and explain a large part of the variance in the trace element records which is not explained by
782 ultradian changes in the animal's behavior.

783 4.4.2 Short-term environmental changes and paleoweather

784 Outside of regular fluctuations caused by tidal, daily and seasonal cycles, changes in light and
785 food availability at the hourly to daily scale are probably linked to circulation and weather
786 phenomena. Previous studies show that enhanced vertical mixing during weather events such as
787 storms, algal bloom events after wind-driven upwelling and pseudoperiodic dust deposition can
788 temporarily increase the concentration of dissolved metals in surface waters, resuspend organic
789 matter and temporarily increase primary productivity. (Lin et al., 2003; Al-Najjar et al., 2007; Iluz
790 et al., 2009; Al-Taani et al., 2015; Komagoe et al., 2018). This will in turn lead to a shallowing of
791 the redoxcline through increased organic matter load at the sediment-water interface, which can
792 be recorded in the composition of giant clam shells (Yan et al., 2020). Interestingly, data in Yan
793 et al. (2020) suggest that recording an extreme weather event in *Tridacna* requires wind speeds
794 exceeding 20 km/h, a threshold which is almost never reached in the comparatively quiet Gulf of
795 Aqaba (Manasrah et al., 2019), while such events are common in the stormier Bay of Brest (Hily
796 et al., 1992; Chauvaud et al., 1998). This highlights another difference between the environments
797 of pectinid and tridacnid specimens investigated in this study which could contribute to the
798 variable expression of periodicity in the trace element composition of their shells. A plausible
799 scenario therefore emerges in which aperiodic weather events cause short-term variability in both
800 the chemistry and physical properties of the water column. These changes are subsequently
801 recorded in bivalve shells, either directly because the weather events resuspend, remobilize or
802 deliver trace elements like Mn and Ba (e.g., Dehairs et al., 1989; Gillikin et al., 2008; Mahé et al.,
803 2010), or indirectly because environmental stress associated with the event affects behavior and



804 shell calcification, resulting in a change in the incorporation of alkali-group cations (e.g., Mg and
805 Sr) into the shell biomineral (Carré et al., 2006; Takesue et al., 2008; **Fig. 7**). Our results therefore
806 highlight the potential of high-resolution trace element records in bivalve shells to record short-
807 term circulation changes and weather events, while prescribing caution in interpreting such
808 records until the effect of true environmental changes on the sub-daily scale can be separated
809 from aperiodic ultradian or behavioral patterns.

810



811 **5. Conclusions**

812 Our high-resolution trace element records reveal that short-term variability on the tidal or daily
813 scale is recorded in the Mg, Sr, Mn, and Ba composition of shells of fast-growing mollusk species.
814 The application of spectral analysis and variance decomposition on these trace element records
815 is a useful tool to assess the influence of periodicity in the shallow marine environment on
816 calcification in mollusk shells. Our statistical analysis reveals that tidal and daily variability each
817 account for less than 10% of trace element variance in pectinids and tridacnids. In photosymbiotic
818 giant clam shells, the amount of variance in Sr and Ba paced to the daily cycle is two times higher
819 than in the non-photosymbiotic pectinids, suggesting that photosymbiosis in giant clams exerts
820 some control on trace element composition in their shells. However, since only ~10% of the trace
821 element variability in tridacnids is explained by diurnal variability, the recognition of
822 photosymbiosis in the fossil record from diurnal variability in fossil shell composition will be
823 complicated. In addition, differences between the mid-latitude environment of the pectinids and
824 the tropical environment of the tridacnids likely account for part of the difference in trace element
825 composition between the taxa. We propose that Ba and Mn composition in pectinids and
826 tridacnids reflect short-term variability in primary productivity and sea water chemistry which
827 control the mobility of these elements. Concentrations of Mg and Sr are likely controlled by short-
828 term changes in growth and metabolic rate of the mollusks, which may be indirectly controlled by
829 changes in their environment through circadian rhythms or behavior, explaining the pacing of
830 trace element composition to the tidal and diurnal cycle. Most of the variance in trace element
831 records in both taxa are not related to periodic behavior at the 12h or 24h scale, likely recording
832 aperiodic events in the environment related to weather-scale phenomena or circadian patterns.
833 We thus conclude that mollusk shell carbonate is a promising archive for recording weather-scale
834 variability in shallow marine environments across latitudes, potentially recording weather-scale



835 phenomena in deep time, as long as these environmental effects can be separated by the
836 influence of the animal's behavior.

837

838 **Code availability**

839 Scripts used for data processing and to create figures in this manuscript were uploaded to an
840 open-access repository on GitHub (https://github.com/nielsjdewinter/TE_circadian) and linked
841 through Zenodo (<https://zenodo.org/record/6603175>).

842

843 **Data availability**

844 Supplementary data and figures referenced in this contribution were uploaded to the online open-
845 access repository Zenodo (<https://doi.org/10.5281/zenodo.6602894>).

846

847 **Author contribution**

848 NJW designed the experiment after discussion with BRS, DK and LF. LF, DK, BRS and JT
849 collected the samples. LF, DK and NJW together prepared samples for analyses and constructed
850 shell chronologies using growth line counting. WB, LN, GJR and NJW carried out the LA-ICP-MS
851 analyses and data processing. NJW designed and carried out the statistical analyses and wrote
852 the R scripts guided by feedback from LN, BK, LN, WB and GJR. NJW wrote the first draft of the
853 manuscript. All authors contributed to the writing process towards the final version of the
854 manuscript.

855

856 **Competing interests**



857 The authors declare that they have no conflict of interest.

858 **Acknowledgements**

859 The authors would like to thank Leonard Bik for his help with sample preparation and Maarten
860 Zeilmans for his help with high-resolution imaging of the samples at Utrecht University. This study
861 is part of the UNBIAS project, jointly funded by a Flemish Research Foundation (FWO;
862 12ZB220N) post-doctoral fellowship (NJW) and a MSCA Individual Fellowship (H2020-MSCA-IF-
863 2018; 843011 – UNBIAS; awarded to NJW). GJR and LKD acknowledge funding from the
864 Netherlands Earth System Science Center (NESSC; grant no. 024.002.001) from the Dutch
865 Ministry for Education, Culture and Science (gravitation grant no. NWO 024.002.001). BRS
866 acknowledges funding from the Deutsche Forschungsgemeinschaft (DFG; SCHO/793/21). JT
867 acknowledges funding from the French National Research Agency (ANR; ANR-18-CE92-0036-
868 01) awarded within the framework of the French-German collaborative project HIPPO (High-
869 resolution Primary Production multiprOxy archives).

870

871 **References**

- 872 Agbaje, O. B. A., Wirth, R., Morales, L. F. G., Shirai, K., Kosnik, M., Watanabe, T., and Jacob,
873 D. E.: Architecture of crossed-lamellar bivalve shells: the southern giant clam (*Tridacna derasa*,
874 Röding, 1798), 4, 170622, <https://doi.org/10.1098/rsos.170622>, n.d.
- 875 Al-Aasm, I. S. and Veizer, J.: Diagenetic Stabilization of Aragonite and Low-mg Calcite, I. Trace
876 Elements in Rudists, 56, 1986a.
- 877 Al-Aasm, I. S. and Veizer, J.: Diagenetic stabilization of aragonite and low-Mg calcite, II. Stable
878 isotopes in rudists, 56, 1986b.
- 879 Al-Najjar, T., Badran, M. I., Richter, C., Meyerhoefer, M., and Sommer, U.: Seasonal dynamics
880 of phytoplankton in the Gulf of Aqaba, Red Sea, *Hydrobiologia*, 579, 69–83,
881 <https://doi.org/10.1007/s10750-006-0365-z>, 2007.
- 882 Al-Taani, A. A., Rashdan, M., and Khashashneh, S.: Atmospheric dry deposition of mineral dust
883 to the Gulf of Aqaba, Red Sea: Rate and trace elements, *Marine Pollution Bulletin*, 92, 252–258,
884 <https://doi.org/10.1016/j.marpolbul.2014.11.047>, 2015.



- 885 Armstrong, E. J., Roa, J. N., Stillman, J. H., and Tresguerres, M.: Symbiont photosynthesis in
886 giant clams is promoted by V-type H⁺-ATPase from host cells, *Journal of Experimental Biology*,
887 221, jeb177220, <https://doi.org/10.1242/jeb.177220>, 2018.
- 888 Ballesta-Artero, I., Witbaard, R., Carroll, M. L., and van der Meer, J.: Environmental factors
889 regulating gaping activity of the bivalve *Arctica islandica* in Northern Norway, *Mar Biol*, 164, 116,
890 <https://doi.org/10.1007/s00227-017-3144-7>, 2017.
- 891 Barats, A., Amouroux, D., Pécheyran, C., Chauvaud, L., and Donard, O. F. X.: High-Frequency
892 Archives of Manganese Inputs To Coastal Waters (Bay of Seine, France) Resolved by the
893 LA-ICP-MS Analysis of Calcitic Growth Layers along Scallop Shells (*Pecten maximus*),
894 *Environ. Sci. Technol.*, 42, 86–92, <https://doi.org/10.1021/es0701210>, 2008.
- 895 Barats, A., Amouroux, D., Chauvaud, L., Pécheyran, C., Lorrain, A., Thébault, J., Church, T. M.,
896 and Donard, O. F. X.: High frequency Barium profiles in shells of the Great Scallop *Pecten*
897 *maximus*: a methodical long-term and multi-site survey in Western Europe, 6, 157–170,
898 <https://doi.org/10.5194/bg-6-157-2009>, 2009.
- 899 Batenburg, S. J., Reichart, G.-J., Jilbert, T., Janse, M., Wesselingh, F. P., and Renema, W.:
900 Interannual climate variability in the Miocene: High resolution trace element and stable isotope
901 ratios in giant clams, *Palaeogeography, Palaeoclimatology, Palaeoecology*, 306, 75–81,
902 <https://doi.org/10.1016/j.palaeo.2011.03.031>, 2011.
- 903 Black, B. A.: Climate-driven synchrony across tree, bivalve, and rockfish growth-increment
904 chronologies of the northeast Pacific, 378, 37–46, 2009.
- 905 Boo, M. V., Chew, S. F., and Ip, Y. K.: The colorful mantle of the giant clam *Tridacna squamosa*
906 expresses a homolog of electrogenic sodium: Bicarbonate cotransporter 2 that mediates the
907 supply of inorganic carbon to photosynthesizing symbionts, *PLoS One*, 16, e0258519,
908 <https://doi.org/10.1371/journal.pone.0258519>, 2021.
- 909 Bougeois, L., de Rafélis, M., Reichart, G.-J., de Nooijer, L. J., Nicollin, F., and Dupont-Nivet, G.:
910 A high resolution study of trace elements and stable isotopes in oyster shells to estimate Central
911 Asian Middle Eocene seasonality, *Chemical Geology*, 363, 200–212,
912 <https://doi.org/10.1016/j.chemgeo.2013.10.037>, 2014.
- 913 Carlson, D. F., Fredj, E., and Gildor, H.: The annual cycle of vertical mixing and restratification
914 in the Northern Gulf of Eilat/Aqaba (Red Sea) based on high temporal and vertical resolution
915 observations, *Deep Sea Research Part I: Oceanographic Research Papers*, 84, 1–17,
916 <https://doi.org/10.1016/j.dsr.2013.10.004>, 2014.
- 917 Carré, M., Bentaleb, I., Bruguier, O., Ordinola, E., Barrett, N. T., and Fontugne, M.: Calcification
918 rate influence on trace element concentrations in aragonitic bivalve shells: evidences and
919 mechanisms, 70, 4906–4920, 2006.
- 920 Chauvaud, L., Thouzeau, G., and Paulet, Y.-M.: Effects of environmental factors on the daily
921 growth rate of *Pecten maximus* juveniles in the Bay of Brest (France), *Journal of Experimental*
922 *Marine Biology and Ecology*, 227, 83–111, [https://doi.org/10.1016/S0022-0981\(97\)00263-3](https://doi.org/10.1016/S0022-0981(97)00263-3),
923 1998.



- 924 Chauvaud, L., Lorrain, A., Dunbar, R. B., Paulet, Y.-M., Thouzeau, G., Jean, F., Guarini, J.-M.,
925 and Mucciarone, D.: Shell of the Great Scallop *Pecten maximus* as a high-frequency archive of
926 paleoenvironmental changes, 6, <https://doi.org/10.1029/2004GC000890>, 2005.
- 927 Checa, A. G., Esteban-Delgado, F. J., and Rodríguez-Navarro, A. B.: Crystallographic structure
928 of the foliated calcite of bivalves, 157, 393–402, 2007.
- 929 Chew, S. F., Koh, C. Z., Hiong, K. C., Choo, C. Y., Wong, W. P., Neo, M. L., and Ip, Y. K.: Light-
930 enhanced expression of Carbonic Anhydrase 4-like supports shell formation in the fluted giant
931 clam *Tridacna squamosa*, 683, 101–112, 2019.
- 932 Cochran, J. K., Kallenberg, K., Landman, N. H., Harries, P. J., Weinreb, D., Turekian, K. K.,
933 Beck, A. J., and Cobban, W. A.: Effect of diagenesis on the Sr, O, and C isotope composition of
934 late Cretaceous mollusks from the Western Interior Seaway of North America, 310, 69–88,
935 <https://doi.org/10.2475/02.2010.01>, 2010.
- 936 Cohen, A. L., Owens, K. E., Layne, G. D., and Shimizu, N.: The Effect of Algal Symbionts on the
937 Accuracy of Sr/Ca Paleotemperatures from Coral, 296, 331–333,
938 <https://doi.org/10.1126/science.1069330>, 2002.
- 939 Coimbra, R., Huck, S., de Winter, N. J., Heimhofer, U., and Claeys, P.: Improving the detection
940 of shell alteration: Implications for sclerochronology, *Palaeogeography, Palaeoclimatology,*
941 *Palaeoecology*, 559, 109968, <https://doi.org/10.1016/j.palaeo.2020.109968>, 2020.
- 942 Comboul, M., Emile-Geay, J., Evans, M. N., Mirnateghi, N., Cobb, K. M., and Thompson, D. M.:
943 A probabilistic model of chronological errors in layer-counted climate proxies: applications to
944 annually banded coral archives, 10, 825–841, 2014.
- 945 Crippa, G., Grieshaber, E., Checa, A. G., Harper, E. M., Roda, M. S., and Schmahl, W. W.:
946 Orientation patterns of aragonitic crossed-lamellar, fibrous prismatic and myostracal
947 microstructures of modern *Glycymeris* shells, 212, 107653, 2020.
- 948 Dauphin, Y., Cuif, J., Doucet, J., Salomé, M., Susini, J., and Williams, C.: In situ mapping of
949 growth lines in the calcitic prismatic layers of mollusc shells using X-ray absorption near-edge
950 structure (XANES) spectroscopy at the sulphur K-edge, *Marine Biology*, 142, 299–304,
951 <https://doi.org/10.1007/s00227-002-0950-2>, 2003.
- 952 DeCarlo, T. M. and Cohen, A. L.: Dissepiments, density bands and signatures of thermal stress
953 in *Porites* skeletons, *Coral Reefs*, 36, 749–761, <https://doi.org/10.1007/s00338-017-1566-9>,
954 2017.
- 955 Dehairs, F., Baeyens, W., and Van Gansbeke, D.: Tight coupling between enrichment of iron
956 and manganese in North Sea suspended matter and sedimentary redox processes: Evidence
957 for seasonal variability, *Estuarine, Coastal and Shelf Science*, 29, 457–471,
958 [https://doi.org/10.1016/0272-7714\(89\)90080-2](https://doi.org/10.1016/0272-7714(89)90080-2), 1989.
- 959 Dunbar, R. B. and Wellington, G. M.: Stable isotopes in a branching coral monitor seasonal
960 temperature variation, 293, 453–455, 1981.
- 961 Elliot, M., Welsh, K., Chilcott, C., McCulloch, M., Chappell, J., and Ayling, B.: Profiles of trace
962 elements and stable isotopes derived from giant long-lived *Tridacna gigas* bivalves: Potential



- 963 applications in paleoclimate studies, *Palaeogeography, Palaeoclimatology, Palaeoecology*, 280,
964 132–142, <https://doi.org/10.1016/j.palaeo.2009.06.007>, 2009.
- 965 Freitas, P. S., Clarke, L. J., Kennedy, H., and Richardson, C. A.: Ion microprobe assessment of
966 the heterogeneity of Mg/Ca, Sr/Ca and Mn/Ca ratios in *Pecten maximus* and *Mytilus edulis*
967 (bivalvia) shell calcite precipitated at constant temperature, 6, 1209–1227,
968 <https://doi.org/10.5194/bg-6-1209-2009>, 2009.
- 969 Fröhlich, L., Siebert, V., Walliser, E. O., Thébault, J., Jochum, K. P., Chauvaud, L., and Schöne,
970 B. R.: Ba/Ca profiles in shells of *Pecten maximus* – A proxy for specific primary producers rather
971 than bulk phytoplankton, *Chemical Geology*, 120743,
972 <https://doi.org/10.1016/j.chemgeo.2022.120743>, 2022.
- 973 Gannon, M. E., Pérez-Huerta, A., Aharon, P., and Street, S. C.: A biomineralization study of the
974 Indo-Pacific giant clam *Tridacna gigas*, *Coral Reefs*, 36, 503–517,
975 <https://doi.org/10.1007/s00338-016-1538-5>, 2017.
- 976 García-March, J. R., Sanchís Solsona, M. Á., and García-Carrascosa, A. M.: Shell gaping
977 behaviour of *Pinna nobilis* L., 1758: circadian and circalunar rhythms revealed by in situ
978 monitoring, *Mar Biol*, 153, 689–698, <https://doi.org/10.1007/s00227-007-0842-6>, 2008.
- 979 Gilbert, P. U., Bergmann, K. D., Myers, C. E., Marcus, M. A., DeVol, R. T., Sun, C.-Y., Blonsky,
980 A. Z., Tamre, E., Zhao, J., and Karan, E. A.: Nacre tablet thickness records formation
981 temperature in modern and fossil shells, 460, 281–292, 2017.
- 982 Gillikin, D. P., Lorrain, A., Paulet, Y.-M., André, L., and Dehairs, F.: Synchronous barium peaks
983 in high-resolution profiles of calcite and aragonite marine bivalve shells, *Geo-Mar Lett*, 28, 351–
984 358, <https://doi.org/10.1007/s00367-008-0111-9>, 2008.
- 985 Goodwin, D. H., Paul, P., and Wissink, C. L.: MoGroFunGen: A numerical model for
986 reconstructing intra-annual growth rates of bivalve molluscs, *Palaeogeography,*
987 *Palaeoclimatology, Palaeoecology*, 276, 47–55, <https://doi.org/10.1016/j.palaeo.2009.02.026>,
988 2009.
- 989 Guillaume Olivier, M., Leroux, E., Rabineau, M., Le Hir, P., Granjeon, D., Chataigner, T.,
990 Beudin, A., and Muller, H.: Numerical modelling of a Macrotidal Bay over the last 9,000 years:
991 An interdisciplinary methodology to understand the influence of sea-level variations on tidal
992 currents in the Bay of Brest, *Continental Shelf Research*, 231, 104595,
993 <https://doi.org/10.1016/j.csr.2021.104595>, 2021.
- 994 Guillong, M., Meier, D. L., Allan, M. M., Heinrich, C. A., and Yardley, B. W. D.: M.GUILLONG,
995 D.L. MEIER, M.M. ALLAN, C.A. HEINRICH & B.W.D. YARDLEY, 40, 328–333, 2008.
- 996 Hily, C., Potin, P., and Floc'h, J.-Y.: Structure of subtidal algal assemblages on soft-bottom
997 sediments: fauna/flora interactions and role of disturbances in the Bay of Brest, France, 85,
998 115–130, 1992.
- 999 Höche, N., Peharda, M., Walliser, E. O., and Schöne, B. R.: Morphological variations of
1000 crossed-lamellar ultrastructures of *Glycymeris bimaculata* (Bivalvia) serve as a marine
1001 temperature proxy, 237, 106658, 2020.



- 1002 Höche, N., Walliser, E. O., de Winter, N. J., Witbaard, R., and Schöne, B. R.: Temperature-
1003 induced microstructural changes in shells of laboratory-grown *Arctica islandica* (Bivalvia), 16,
1004 e0247968, 2021.
- 1005 Huyghe, D., de Rafelis, M., Ropert, M., Mouchi, V., Emmanuel, L., Renard, M., and Lartaud, F.:
1006 New insights into oyster high-resolution hinge growth patterns, 166, 48, 2019.
- 1007 Huyghe, D., Daëron, M., de Rafelis, M., Blamart, D., Sébilo, M., Paulet, Y.-M., and Lartaud, F.:
1008 Clumped isotopes in modern marine bivalves, *Geochimica et Cosmochimica Acta*,
1009 <https://doi.org/10.1016/j.gca.2021.09.019>, 2021.
- 1010 Iluz, D., Dishon, G., Capuzzo, E., Meeder, E., Astoreca, R., Montecino, V., Znachor, P., Ediger,
1011 D., and Marra, J.: Short-term variability in primary productivity during a wind-driven diatom
1012 bloom in the Gulf of Eilat (Aqaba), 56, 205–215, <https://doi.org/10.3354/ame01321>, 2009.
- 1013 Inoue, M., Nakamura, T., Tanaka, Y., Suzuki, A., Yokoyama, Y., Kawahata, H., Sakai, K., and
1014 Gussone, N.: A simple role of coral-algal symbiosis in coral calcification based on multiple
1015 geochemical tracers, *Geochimica et Cosmochimica Acta*, 235, 76–88,
1016 <https://doi.org/10.1016/j.gca.2018.05.016>, 2018.
- 1017 Ip, Y. K. and Chew, S. F.: Light-Dependent Phenomena and Related Molecular Mechanisms in
1018 Giant Clam-Dinoflagellate Associations: A Review, 8, 2021.
- 1019 Ip, Y. K., Loong, A. M., Hiong, K. C., Wong, W. P., Chew, S. F., Reddy, K., Sivaloganathan, B.,
1020 and Ballantyne, J. S.: Light induces an increase in the pH of and a decrease in the ammonia
1021 concentration in the extrapallial fluid of the giant clam *Tridacna squamosa*, 79, 656–664, 2006.
- 1022 Ip, Y. K., Koh, C. Z., Hiong, K. C., Choo, C. Y., Boo, M. V., Wong, W. P., Neo, M. L., and Chew,
1023 S. F.: Carbonic anhydrase 2-like in the giant clam, *Tridacna squamosa*: characterization,
1024 localization, response to light, and possible role in the transport of inorganic carbon from the
1025 host to its symbionts, 5, e13494, 2017.
- 1026 Ivany, L. C.: Reconstructing paleoseasonality from accretionary skeletal carbonates—
1027 challenges and opportunities, 18, 133–166, 2012.
- 1028 Ivany, L. C. and Judd, E. J.: Deciphering Temperature Seasonality in Earth's Ancient Oceans,
1029 50, 123–152, <https://doi.org/10.1146/annurev-earth-032320-095156>, 2022.
- 1030 Jablonski, D., Roy, K., Valentine, J. W., Price, R. M., and Anderson, P. S.: The Impact of the
1031 Pull of the Recent on the History of Marine Diversity, 300, 1133–1135,
1032 <https://doi.org/10.1126/science.1083246>, 2003.
- 1033 Jablonski, D., Huang, S., Roy, K., and Valentine, J. W.: Shaping the latitudinal diversity
1034 gradient: new perspectives from a synthesis of paleobiology and biogeography, 189, 1–12,
1035 2017.
- 1036 Jochum, K. P., Nohl, U., Herwig, K., Lammel, E., Stoll, B., and Hofmann, A. W.: GeoReM: A
1037 New Geochemical Database for Reference Materials and Isotopic Standards, 29, 333–338,
1038 <https://doi.org/10.1111/j.1751-908X.2005.tb00904.x>, 2005.
- 1039 Jochum, K. P., Weis, U., Stoll, B., Kuzmin, D., Yang, Q., Raczek, I., Jacob, D. E., Stracke, A.,
1040 Birbaum, K., Frick, D. A., Günther, D., and Enzweiler, J.: Determination of Reference Values for



- 1041 NIST SRM 610–617 Glasses Following ISO Guidelines, 35, 397–429,
1042 <https://doi.org/10.1111/j.1751-908X.2011.00120.x>, 2011.
- 1043 Jones, D. S.: Sclerochronology: reading the record of the molluscan shell: annual growth
1044 increments in the shells of bivalve molluscs record marine climatic changes and reveal
1045 surprising longevity, 71, 384–391, 1983.
- 1046 Jones, D. S. and Quitmyer, I. R.: Marking Time with Bivalve Shells: Oxygen Isotopes and
1047 Season of Annual Increment Formation, *PALAIOS*, 11, 340–346,
1048 <https://doi.org/10.2307/3515244>, 1996.
- 1049 Judd, E. J., Wilkinson, B. H., and Ivany, L. C.: The life and time of clams: Derivation of intra-
1050 annual growth rates from high-resolution oxygen isotope profiles, *Palaeogeography*,
1051 *Palaeoclimatology*, *Palaeoecology*, <https://doi.org/10.1016/j.palaeo.2017.09.034>, 2017.
- 1052 Killam, D., Thomas, R., Al-Najjar, T., and Clapham, M.: Interspecific and Intrashell Stable
1053 Isotope Variation Among the Red Sea Giant Clams, 21, e2019GC008669,
1054 <https://doi.org/10.1029/2019GC008669>, 2020.
- 1055 Killam, D. E. and Clapham, M. E.: Identifying the ticks of bivalve shell clocks: Seasonal growth
1056 in relation to temperature and food supply, *PALAIOS*, 33, 228–236,
1057 <https://doi.org/10.2110/palo.2017.072>, 2018.
- 1058 Klein, R. T., Lohmann, K. C., and Thayer, C. W.: Bivalve skeletons record sea-surface
1059 temperature and $\delta^{18}\text{O}$ via Mg/Ca and $18\text{O}/16\text{O}$ ratios, 24, 415–418, 1996.
- 1060 Komagoe, T., Watanabe, T., Shirai, K., Yamazaki, A., and Uematu, M.: Geochemical and
1061 Microstructural Signals in Giant Clam *Tridacna maxima* Recorded Typhoon Events at Okinotori
1062 Island, Japan, 123, 1460–1474, <https://doi.org/10.1029/2017JG004082>, 2018.
- 1063 Kontoyannis, C. G. and Vagenas, N. V.: Calcium carbonate phase analysis using XRD and FT-
1064 Raman spectroscopy, *Analyst*, 125, 251–255, <https://doi.org/10.1039/A908609I>, 2000.
- 1065 Ku, H. H.: Notes on the use of propagation of error formulas, 70, 263–273, 1966.
- 1066 Lazareth, C. E., Vander Putten, E., André, L., and Dehairs, F.: High-resolution trace element
1067 profiles in shells of the mangrove bivalve *Isognomon ephippium*: a record of environmental
1068 spatio-temporal variations?, 57, 1103–1114, 2003.
- 1069 Lazareth, C. E., Guzman, N., Poitrasson, F., Candaudap, F., and Ortlieb, L.: Nyctemeral
1070 variations of magnesium intake in the calcitic layer of a Chilean mollusk shell (*Concholepas*
1071 *concholepas*, *Gastropoda*), *Geochimica et Cosmochimica Acta*, 71, 5369–5383,
1072 <https://doi.org/10.1016/j.gca.2007.07.031>, 2007.
- 1073 LAZIER, A. V., SMITH, J. E., RISK, M. J., and SCHWARCZ, H. P.: The skeletal structure of
1074 *Desmophyllum cristagalli*: the use of deep-water corals in sclerochronology, 32, 119–130, 1999.
- 1075 Lin, I., Liu, W. T., Wu, C.-C., Wong, G. T. F., Hu, C., Chen, Z., Liang, W.-D., Yang, Y., and Liu,
1076 K.-K.: New evidence for enhanced ocean primary production triggered by tropical cyclone, 30,
1077 <https://doi.org/10.1029/2003GL017141>, 2003.



- 1078 Lorrain, A., Gillikin, D. P., Paulet, Y.-M., Chauvaud, L., Le Mercier, A., Navez, J., and André, L.:
1079 Strong kinetic effects on Sr/Ca ratios in the calcitic bivalve *Pecten maximus*, *Geology*, 33, 965–
1080 968, <https://doi.org/10.1130/G22048.1>, 2005.
- 1081 Lough, J. M.: Climate records from corals, 1, 318–331, <https://doi.org/10.1002/wcc.39>, 2010.
- 1082 Madkour, H. A.: Distribution and relationships of heavy metals in the giant clam (*Tridacna*
1083 *maxima*) and associated sediments from different sites in the Egyptian Red Sea Coast, توزيع
1084 وعلاقات العناصر الثقيلة في الكائن الصدفي الكبير (نراى داكنا مكسيما (والرواسب المصاحبة من مناطق مختلفة للساحل المصرى
1085 للبحر الاحمر, 2005.
- 1086 Mahé, K., Bellamy, E., Lartaud, F., and Rafélis, M. de: Calcein and manganese experiments for
1087 marking the shell of the common cockle (*Cerastoderma edule*): tidal rhythm validation of
1088 increments formation, *Aquat. Living Resour.*, 23, 239–245, <https://doi.org/10.1051/alr/2010025>,
1089 2010.
- 1090 Manasrah, R., Abu-Hilal, A., and Rasheed, M.: Physical and Chemical Properties of Seawater in
1091 the Gulf of Aqaba and Red Sea, in: *Oceanographic and Biological Aspects of the Red Sea*,
1092 edited by: Rasul, N. M. A. and Stewart, I. C. F., Springer International Publishing, Cham, 41–73,
1093 https://doi.org/10.1007/978-3-319-99417-8_3, 2019.
- 1094 Marin, F. and Luquet, G.: Molluscan shell proteins, *Comptes Rendus Palevol*, 3, 469–492,
1095 <https://doi.org/10.1016/j.crpv.2004.07.009>, 2004.
- 1096 Mat, A. M., Sarrazin, J., Markov, G. V., Apremont, V., Dubreuil, C., Eché, C., Fabioux, C., Klopp,
1097 C., Sarradin, P.-M., Tanguy, A., Huvet, A., and Matabos, M.: Biological rhythms in the deep-sea
1098 hydrothermal mussel *Bathymodiolus azoricus*, *Nat Commun*, 11, 3454,
1099 <https://doi.org/10.1038/s41467-020-17284-4>, 2020.
- 1100 Meibom, A., Stage, M., Wooden, J., Constantz, B. R., Dunbar, R. B., Owen, A., Grumet, N.,
1101 Bacon, C. R., and Chamberlain, C. P.: Monthly Strontium/Calcium oscillations in symbiotic coral
1102 aragonite: Biological effects limiting the precision of the paleotemperature proxy, 30,
1103 <https://doi.org/10.1029/2002GL016864>, 2003.
- 1104 Meyers, S. R.: Seeing red in cyclic stratigraphy: Spectral noise estimation for astrochronology,
1105 27, 2012.
- 1106 Meyers, S. R.: Astrochron: An R package for astrochronology, [http://cran.r-](http://cran.r-project.org/package=astrochron)
1107 [project.org/package=astrochron](http://cran.r-project.org/package=astrochron), 2014.
- 1108 Mohammed, T. A. A., Mohamed, M. H., Zamzamy, R. M., and Mahmoud, M. A. M.: Growth rates
1109 of the giant clam *Tridacna maxima* (Röding, 1798) reared in cages in the Egyptian Red Sea,
1110 *The Egyptian Journal of Aquatic Research*, 45, 67–73,
1111 <https://doi.org/10.1016/j.ejar.2019.02.003>, 2019.
- 1112 Munro, J. L.: Estimation of the parameters of the von Bertalanffy growth equation from recapture
1113 data at variable time intervals, *ICES Journal of Marine Science*, 40, 199–200,
1114 <https://doi.org/10.1093/icesjms/40.2.199>, 1982.
- 1115 Nassar, M. Z., Mohamed, H. R., Khiray, H. M., and Rashedy, S. H.: Seasonal fluctuations of
1116 phytoplankton community and physico-chemical parameters of the north western part of the



- 1117 Red Sea, Egypt, The Egyptian Journal of Aquatic Research, 40, 395–403,
1118 <https://doi.org/10.1016/j.ejar.2014.11.002>, 2014.
- 1119 Onuma, N., Masuda, F., Hirano, M., and Wada, K.: Crystal structure control on trace element
1120 partition in molluscan shell formation, 13, 187–189, <https://doi.org/10.2343/geochemj.13.187>,
1121 1979.
- 1122 Pandolfi, J. M. and Kiessling, W.: Gaining insights from past reefs to inform understanding of
1123 coral reef response to global climate change, Current Opinion in Environmental Sustainability, 7,
1124 52–58, <https://doi.org/10.1016/j.cosust.2013.11.020>, 2014.
- 1125 Pannella, G.: Tidal growth patterns in recent and fossil mollusc bivalve shells: a tool for the
1126 reconstruction of paleotides, 63, 539–543, 1976.
- 1127 Petersen, S. V., Tabor, C. R., Lohmann, K. C., Poulsen, C. J., Meyer, K. W., Carpenter, S. J.,
1128 Erickson, J. M., Matsunaga, K. K., Smith, S. Y., and Sheldon, N. D.: Temperature and salinity of
1129 the Late Cretaceous western interior seaway, 44, 903–906, 2016.
- 1130 Poitevin, P., Chauvaud, L., Pécheyran, C., Lazure, P., Jolivet, A., and Thébault, J.: Does trace
1131 element composition of bivalve shells record ultra-high frequency environmental variations?,
1132 Marine Environmental Research, 158, 104943,
1133 <https://doi.org/10.1016/j.marenvres.2020.104943>, 2020.
- 1134 Polsenaere, P., Deflandre, B., Thouzeau, G., Rigaud, S., Cox, T., Amice, E., Bec, T. L.,
1135 Bihannic, I., and Maire, O.: Comparison of benthic oxygen exchange measured by aquatic Eddy
1136 Covariance and Benthic Chambers in two contrasting coastal biotopes (Bay of Brest, France),
1137 Regional Studies in Marine Science, 43, 101668, <https://doi.org/10.1016/j.rsma.2021.101668>,
1138 2021.
- 1139 Popov, S. V.: Formation of bivalve shells and their microstructure, 48, 1519–1531,
1140 <https://doi.org/10.1134/S003103011414010X>, 2014.
- 1141 R Core Team: R: A Language and Environment for Statistical Computing, R Foundation for
1142 Statistical Computing, Vienna, Austria, 2022.
- 1143 Richard, M.: Analyse de la composition élémentaire de *Pecten maximus* par HR-ICP-MS
1144 Element 2: développements méthodologiques et interprétations écologiques., PhD Thesis,
1145 Université de Bretagne occidentale-Brest, 264 pp, 2009.
- 1146 Richardson, C. A., Crisp, D. J., Runham, N. W., and Gruffydd, L. D.: The use of tidal growth
1147 bands in the shell of *Cerastoderma edule* to measure seasonal
1148 growth rates under cool temperate and sub-arctic conditions, 60, 977–989,
1149 <https://doi.org/10.1017/S002531540004203X>, 1980.
- 1150 Richter, C., Roa-Quiaoit, H., Jantzen, C., Al-Zibdah, M., and Kochzius, M.: Collapse of a new
1151 living species of giant clam in the Red Sea, 18, 1349–1354, 2008.
- 1152 Roa-Quiaoit, H.: Ecology and culture of giant clams (Tridacnidae) in the Jordanian sector of the
1153 Gulf of Aqaba, Red Sea, http://elib.suub.uni-bremen.de/diss/docs/E-Diss1340_PHDRQAQ.pdf,
1154 2005.



- 1155 Roberts, E. M., Bowers, D. G., and Davies, A. J.: Tidal modulation of seabed light and its
1156 implications for benthic algae, 63, 91–106, <https://doi.org/10.1002/lno.10616>, 2018.
- 1157 Robson, A. A., Chauvaud, L., Wilson, R. P., and Halsey, L. G.: Small actions, big costs: the
1158 behavioural energetics of a commercially important invertebrate, 9, 1486–1498,
1159 <https://doi.org/10.1098/rsif.2011.0713>, 2012.
- 1160 Rodland, D. L., Schöne, B. R., Helama, S., Nielsen, J. K., and Baier, S.: A clockwork mollusc:
1161 Ultradian rhythms in bivalve activity revealed by digital photography, *Journal of Experimental*
1162 *Marine Biology and Ecology*, 334, 316–323, <https://doi.org/10.1016/j.jembe.2006.02.012>, 2006.
- 1163 Sano, Y., Kobayashi, S., Shirai, K., Takahata, N., Matsumoto, K., Watanabe, T., Sowa, K., and
1164 Iwai, K.: Past daily light cycle recorded in the strontium/calcium ratios of giant clam shells, *Nat*
1165 *Commun*, 3, 761, <https://doi.org/10.1038/ncomms1763>, 2012.
- 1166 Schöne, B. R. and Giere, O.: Growth increments and stable isotope variation in shells of the
1167 deep-sea hydrothermal vent bivalve mollusk *Bathymodiolus brevior* from the North Fiji Basin,
1168 *Pacific Ocean*, 52, 1896–1910, 2005.
- 1169 Schöne, B. R. and Gillikin, D. P.: Unraveling environmental histories from skeletal diaries —
1170 *Advances in sclerochronology, Palaeogeography, Palaeoclimatology, Palaeoecology*, 373, 1–5,
1171 <https://doi.org/10.1016/j.palaeo.2012.11.026>, 2013.
- 1172 Schöne, B. R., Castro, A. D. F., Fiebig, J., Houk, S. D., Oschmann, W., and Kröncke, I.: Sea
1173 surface water temperatures over the period 1884–1983 reconstructed from oxygen isotope
1174 ratios of a bivalve mollusk shell (*Arctica islandica*, southern North Sea), 212, 215–232, 2004.
- 1175 Schöne, B. R., Fiebig, J., Pfeiffer, M., Gleß, R., Hickson, J., Johnson, A. L., Dreyer, W., and
1176 Oschmann, W.: Climate records from a bivalved *Methuselah* (*Arctica islandica*, Mollusca;
1177 Iceland), 228, 130–148, 2005a.
- 1178 Schöne, B. R., Houk, S. D., Castro, A. D. F., Fiebig, J., Oschmann, W., Kröncke, I., Dreyer, W.,
1179 and Gosselck, F.: Daily growth rates in shells of *Arctica islandica*: assessing sub-seasonal
1180 environmental controls on a long-lived bivalve mollusk, 20, 78–92, 2005b.
- 1181 Schöne, B. R., Dunca, E., Fiebig, J., and Pfeiffer, M.: Mutvei's solution: An ideal agent for
1182 resolving microgrowth structures of biogenic carbonates, *Palaeogeography, Palaeoclimatology,*
1183 *Palaeoecology*, 228, 149–166, <https://doi.org/10.1016/j.palaeo.2005.03.054>, 2005c.
- 1184 Schöne, B. R., Zhang, Z., Jacob, D., Gillikin, D. P., Tütken, T., Garbe-Schönberg, D.,
1185 McConnaughey, T., and Soldati, A.: Effect of organic matrices on the determination of the trace
1186 element chemistry (Mg, Sr, Mg/Ca, Sr/Ca) of aragonitic bivalve shells (*Arctica islandica*)—
1187 Comparison of ICP-OES and LA-ICP-MS data, 44, 23–37,
1188 <https://doi.org/10.2343/geochemj.1.0045>, 2010.
- 1189 Schwartzmann, C., Durrieu, G., Sow, M., Ciret, P., Lazareth, C. E., and Massabuau, J.-C.: In
1190 situ giant clam growth rate behavior in relation to temperature: A one-year coupled study of
1191 high-frequency noninvasive valvometry and sclerochronology, 56, 1940–1951,
1192 <https://doi.org/10.4319/lo.2011.56.5.1940>, 2011.
- 1193 Service Hydrographique et Océanographique de la Marine, Géoportail:
1194 <https://www.geoportail.gouv.fr/>, last access: 28 June 2022.



- 1195 Sinclair, D. J., Kinsley, L. P. J., and McCulloch, M. T.: High resolution analysis of trace elements
1196 in corals by laser ablation ICP-MS, *Geochimica et Cosmochimica Acta*, 62, 1889–1901,
1197 [https://doi.org/10.1016/S0016-7037\(98\)00112-4](https://doi.org/10.1016/S0016-7037(98)00112-4), 1998.
- 1198 Soldati, A. L., Jacob, D. E., Glatzel, P., Swarbrick, J. C., and Geck, J.: Element substitution by
1199 living organisms: the case of manganese in mollusc shell aragonite, 6, 1–9, 2016.
- 1200 Soo, P. and Todd, P. A.: The behaviour of giant clams (*Bivalvia: Cardiidae: Tridacninae*), *Mar*
1201 *Biol*, 161, 2699–2717, <https://doi.org/10.1007/s00227-014-2545-0>, 2014.
- 1202 Surge, D., Lohmann, K. C., and Dettman, D. L.: Controls on isotopic chemistry of the American
1203 oyster, *Crassostrea virginica*: implications for growth patterns, *Palaeogeography,*
1204 *Palaeoclimatology, Palaeoecology*, 172, 283–296, [https://doi.org/10.1016/S0031-](https://doi.org/10.1016/S0031-0182(01)00303-0)
1205 [0182\(01\)00303-0](https://doi.org/10.1016/S0031-0182(01)00303-0), 2001.
- 1206 Takesue, R. K., Bacon, C. R., and Thompson, J. K.: Influences of organic matter and
1207 calcification rate on trace elements in aragonitic estuarine bivalve shells, *Geochimica et*
1208 *Cosmochimica Acta*, 72, 5431–5445, <https://doi.org/10.1016/j.gca.2008.09.003>, 2008.
- 1209 Tanaka, K., Okaniwa, N., Miyaji, T., Murakami-Sugihara, N., Zhao, L., Tanabe, K., Schöne, B.
1210 R., and Shirai, K.: Microscale magnesium distribution in shell of the Mediterranean mussel
1211 *Mytilus galloprovincialis*: An example of multiple factors controlling Mg/Ca in biogenic calcite,
1212 *Chemical Geology*, 511, 521–532, <https://doi.org/10.1016/j.chemgeo.2018.10.025>, 2019.
- 1213 Taylor, J. D. and Layman, M.: The mechanical properties of bivalve (Mollusca) shell structures,
1214 15, 73–87, 1972.
- 1215 Thébault, J., Chauvaud, L., L’Helguen, S., Clavier, J., Barats, A., Jacquet, Sé., PÉcheyran, C.,
1216 and Amouroux, D.: Barium and molybdenum records in bivalve shells: Geochemical proxies for
1217 phytoplankton dynamics in coastal environments?, 54, 1002–1014,
1218 <https://doi.org/10.4319/lo.2009.54.3.1002>, 2009.
- 1219 Thébault, J., Jolivet, A., Waeles, M., Tabouret, H., Sabarot, S., PÉcheyran, C., Leynaert, A.,
1220 Jochum, K. P., Schöne, B. R., Fröhlich, L., Siebert, V., Amice, E., and Chauvaud, L.: Scallop
1221 shells as geochemical archives of phytoplankton-related ecological processes in a temperate
1222 coastal ecosystem, 67, 187–202, <https://doi.org/10.1002/lno.11985>, 2022.
- 1223 Thomson, D. J.: Spectrum estimation and harmonic analysis, 70, 1055–1096, 1982.
- 1224 Tierney, J. E., Poulsen, C. J., Montañez, I. P., Bhattacharya, T., Feng, R., Ford, H. L., Hönisch,
1225 B., Inglis, G. N., Petersen, S. V., Sahoo, N., Tabor, C. R., Thirumalai, K., Zhu, J., Burls, N. J.,
1226 Foster, G. L., Goddérís, Y., Huber, B. T., Ivany, L. C., Turner, S. K., Lunt, D. J., McElwain, J. C.,
1227 Mills, B. J. W., Otto-Bliesner, B. L., Ridgwell, A., and Zhang, Y. G.: Past climates inform our
1228 future, 370, <https://doi.org/10.1126/science.aay3701>, 2020.
- 1229 Tran, D., Nadau, A., Durrieu, G., Ciret, P., Parisot, J.-P., and Massabuau, J.-C.: Field
1230 Chronobiology of a Molluscan Bivalve: How the Moon and Sun Cycles Interact to Drive Oyster
1231 Activity Rhythms, 28, 307–317, <https://doi.org/10.3109/07420528.2011.565897>, 2011.
- 1232 Tran, D., Perrigault, M., Ciret, P., and Payton, L.: Bivalve mollusc circadian clock genes can run
1233 at tidal frequency, 287, 20192440, <https://doi.org/10.1098/rspb.2019.2440>, 2020.



- 1234 Vander Putten, E., Dehairs, F., Keppens, E., and Baeyens, W.: High resolution distribution of
1235 trace elements in the calcite shell layer of modern *Mytilus edulis*: environmental and biological
1236 controls, 64, 997–1011, 2000.
- 1237 Vermeij, G. J.: The evolution of molluscan photosymbioses: a critical appraisal, *Biological*
1238 *Journal of the Linnean Society*, 109, 497–511, <https://doi.org/10.1111/bij.12095>, 2013.
- 1239 Von Bertalanffy, L.: Quantitative laws in metabolism and growth, 32, 217–231, 1957.
- 1240 Warter, V. and Müller, W.: Daily growth and tidal rhythms in Miocene and modern giant clams
1241 revealed via ultra-high resolution LA-ICPMS analysis—A novel methodological approach
1242 towards improved sclerochemistry, 465, 362–375, 2017.
- 1243 WARTER, V., MÜLLER, W., WESSELINGH, F. P., TODD, J. A., and RENEMA, W.: LATE
1244 MIOCENE SEASONAL TO SUBDECADAL CLIMATE VARIABILITY IN THE INDO-WEST
1245 PACIFIC (EAST KALIMANTAN, INDONESIA) PRESERVED IN GIANT CLAMS, *PALAIOS*, 30,
1246 66–82, <https://doi.org/10.2110/palo.2013.061>, 2015.
- 1247 Warter, V., Erez, J., and Müller, W.: Environmental and physiological controls on daily trace
1248 element incorporation in *Tridacna crocea* from combined laboratory culturing and ultra-high
1249 resolution LA-ICP-MS analysis, *Palaeogeography, Palaeoclimatology, Palaeoecology*, 496, 32–
1250 47, <https://doi.org/10.1016/j.palaeo.2017.12.038>, 2018.
- 1251 Wilson, S. A., Koenig, A. E., and Orklid, R.: Development of microanalytical reference material
1252 (MACS-3) for LA-ICP-MS analysis of carbonate samples, 72, A1025, 2008.
- 1253 de Winter, N. J.: ShellChron 0.4.0: a new tool for constructing chronologies in accretionary
1254 carbonate archives from stable oxygen isotope profiles, 15, 1247–1267,
1255 <https://doi.org/10.5194/gmd-15-1247-2022>, 2022.
- 1256 de Winter, N. J. and Claeys, P.: Micro X-ray fluorescence (μ XRF) line scanning on Cretaceous
1257 rudist bivalves: A new method for reproducible trace element profiles in bivalve calcite,
1258 *Sedimentology*, 64, 231–251, <https://doi.org/10.1111/sed.12299>, 2017.
- 1259 de Winter, N. J., Goderis, S., Dehairs, F., Jagt, J. W., Fraaije, R. H., Van Malderen, S. J.,
1260 Vanhaecke, F., and Claeys, P.: Tropical seasonality in the late Campanian (late Cretaceous):
1261 Comparison between multiproxy records from three bivalve taxa from Oman, 485, 740–760,
1262 2017.
- 1263 de Winter, N. J., Vellekoop, J., Vorrsselmans, R., Golreihan, A., Soete, J., Petersen, S. V.,
1264 Meyer, K. W., Casadio, S., Speijer, R. P., and Claeys, P.: An assessment of latest Cretaceous
1265 *Pycnodonte vesicularis* (Lamarck, 1806) shells as records for palaeoseasonality: a multi-proxy
1266 investigation, 14, 725–749, 2018.
- 1267 de Winter, N. J., Goderis, S., Malderen, S. J. M. V., Sinnesael, M., Vansteenberge, S., Snoeck,
1268 C., Belza, J., Vanhaecke, F., and Claeys, P.: Subdaily-Scale Chemical Variability in a *Torreites*
1269 *Sanchezi* Rudist Shell: Implications for Rudist Paleobiology and the Cretaceous Day-Night
1270 Cycle, 35, e2019PA003723, <https://doi.org/10.1029/2019PA003723>, 2020.
- 1271 de Winter, N. J., Müller, I. A., Kocken, I. J., Thibault, N., Ullmann, C. V., Farnsworth, A., Lunt, D.
1272 J., Claeys, P., and Ziegler, M.: Absolute seasonal temperature estimates from clumped isotopes



- 1273 in bivalve shells suggest warm and variable greenhouse climate, *Commun Earth Environ*, 2, 1–
1274 8, <https://doi.org/10.1038/s43247-021-00193-9>, 2021a.
- 1275 de Winter, N. J., Agterhuis, T., and Ziegler, M.: Optimizing sampling strategies in high-resolution
1276 paleoclimate records, 17, 1315–1340, <https://doi.org/10.5194/cp-17-1315-2021>, 2021b.
- 1277 Winter, N. J. de, Witbaard, R., Kocken, I. J., Müller, I. A., Guo, J., Goudsmit, B., and Ziegler, M.:
1278 Temperature dependence of clumped isotopes ($\Delta 47$) in aragonite,
1279 <https://doi.org/10.1002/essoar.10511492.1>, 31 May 2022.
- 1280 Wichern, N. M. A., de Winter, N. J., Johnson, A. L. A., Goolaerts, S., Wesselingh, F., Hamers,
1281 M. F. J., Kaskens, P., Claeys, P., Ziegler, M. The potential of high-resolution stable isotope
1282 records in the First sclerochronologic and isotopic analysis of bivalve *Angulus benedeni* shells
1283 to investigate Pliocene seasonality. *Climate of the Past*, In review, 2022
- 1284 Wisshak, M., Correa, M. L., Gofas, S., Salas, C., Taviani, M., Jakobsen, J., and Freiwald, A.:
1285 Shell architecture, element composition, and stable isotope signature of the giant deep-sea
1286 oyster *Neopycnodonte zibrowii* sp. n. from the NE Atlantic, 56, 374–407, 2009.
- 1287 Witbaard, R., Jenness, M. I., Van Der Borg, K., and Ganssen, G.: Verification of annual growth
1288 increments in *Arctica islandica* L. from the North Sea by means of oxygen and carbon isotopes,
1289 *Netherlands Journal of Sea Research*, 33, 91–101, [https://doi.org/10.1016/0077-7579\(94\)90054-X](https://doi.org/10.1016/0077-7579(94)90054-X), 1994.
- 1291 Xing, Q., Zhang, L., Li, Y., Zhu, X., Li, Y., Guo, H., Bao, Z., and Wang, S.: Development of
1292 Novel Cardiac Indices and Assessment of Factors Affecting Cardiac Activity in a Bivalve Mollusc
1293 *Chlamys farreri*, 10, 2019.
- 1294 Yan, H., Shao, D., Wang, Y., and Sun, L.: Sr/Ca profile of long-lived *Tridacna gigas* bivalves
1295 from South China Sea: A new high-resolution SST proxy, *Geochimica et Cosmochimica Acta*,
1296 112, 52–65, <https://doi.org/10.1016/j.gca.2013.03.007>, 2013.
- 1297 Yan, H., Liu, C., An, Z., Yang, W., Yang, Y., Huang, P., Qiu, S., Zhou, P., Zhao, N., Fei, H., Ma,
1298 X., Shi, G., Dodson, J., Hao, J., Yu, K., Wei, G., Yang, Y., Jin, Z., and Zhou, W.: Extreme
1299 weather events recorded by daily to hourly resolution biogeochemical proxies of marine giant
1300 clam shells, *PNAS*, 117, 7038–7043, <https://doi.org/10.1073/pnas.1916784117>, 2020.
- 1301 Yoshimura, T., Tamenori, Y., Kawahata, H., and Suzuki, A.: Fluctuations of sulfate, S-bearing
1302 amino acids and magnesium in a giant clam shell, 11, 3881–3886, <https://doi.org/10.5194/bg-11-3881-2014>, 2014.
- 1304 Zhao, L., Schöne, B. R., and Mertz-Kraus, R.: Controls on strontium and barium incorporation
1305 into freshwater bivalve shells (*Corbicula fluminea*), *Palaeogeography, Palaeoclimatology,*
1306 *Palaeoecology*, 465, 386–394, <https://doi.org/10.1016/j.palaeo.2015.11.040>, 2017.